Field-induced spin-density-wave phases in $(TMTSF)_2ClO_4$ at high magnetic field: Effect of anion ordering

S. Haddad,[1] S. Charfi-Kaddour,[1] M. Héritier,[2] and R. Bennaceur[1]
[1]*Laboratoire de Physique de la Matière Condensée, Département de Physique, Faculté des Sciences de Tunis, Campus universitaire 1060 Tunis, Tunisia*
[2]*Laboratoire de Physique des Solides d'Orsay U.M.R. 8502 (unité mixte de Recherche) CNRS-Paris XI, France*
(Received 22 February 2005; revised manuscript received 23 May 2005; published 2 August 2005)

We study the high magnetic field-induced spin-density-wave (FISDW) phases of the relaxed $(TMTSF)_2ClO_4$ salt. Due to an orientational ordering of the ClO_4 anions, a gap opens at the Fermi surface leading to a two band energy spectrum. We go through the different experimental and theoretical results related to the high field regime of the $(TMTSF)_2ClO_4$ phase diagram. We show that, in spite of intensive studies, this phase diagram is still the subject of controversies. We then tackle the issue of analyzing the exotic features of the high field spin-density-wave (SDW) phases. Based on a mean field theory and a renormalization group method, we study the consequences of anion ordering on the stability of the FISFW phases. We show that the presence of a two pairs of Fermi surface gives rise to two types of competing SDW phases. One is due to a single interband nesting process, as in a one band model, while the second originates from two intraband nesting vectors. The latter, for which we derive a generalized instability criterion, has the highest metal-SDW transition temperature and is described by two coexisting order parameters. As the temperature decreases, this coexistence puts at disadvantage the corresponding phase. Eventually, a first order transition takes place to a second SDW phase characterized by a single nesting vector and which appears inside the first one. Within the proposed model, we are able to label the different SDW phases with definite quantum numbers N related to the quantum Hall effect. We argue that the first SDW phase is nothing but the $N=0$ state whereas the inner phase is the $N=1$ state. The obtained results are consistent with recent experiments.

DOI: 10.1103/PhysRevB.72.085104 PACS number(s): 64.60.Ak, 71.10.Pm, 75.30.Fv, 72.15.Gd

I. INTRODUCTION

The quasi-one-dimensional conductors $(TMTSF)_2X$, where TMTSF denotes tetramethyltetraselenafulvalene and the anion $X=PF_6$, ClO_4, ReO_4, etc., present a variety of interesting properties such as superconductivity, quantum Hall effect, rapid oscillations.[1,2] One of the most spectacular properties is the formation of a cascade of magnetic field induced spin density wave (FISDW) phases when a moderate magnetic field (less than 10 T) is applied in the direction perpendicular to the most conducting planes.[3] These phases are characterized by a quantized in-plane Hall resistance $\rho_{xy}=h/2Ne^2$. As the magnetic field increases the integer N varies in the sequence $N=\ldots 4,3,2,1,0$ at each transition between FISDW states. These interphase transitions are of first order while the initial transition from the metallic state to the FISDW state is of second-order. The $N\neq 0$ phases are found to be semimetallic whereas the $N=0$ state is insulating.

In the case of $(TMTSF)_2PF_6$, most of the features of the FISDW cascade, observed under pressure, may be explained within the quantized nesting model (QNM).[4–10] However, it should be stressed that recent magnetoresistance measurements in the $(TMTSF)_2PF_6$ conductor have revealed the presence of low temperature quantum FISDW phases and high-temperature semiclassical FISDW ones.[11] This result is not expected in the QNM but is consistent with a recent model proposed by Lebed.[12] According to the QNM, the metallic state is described, within a Fermi liquid approach, by two slightly warped parallel sheets Fermi surface. The orbital effect of the magnetic field reduces the effective dimensionality of the electron system and, therefore destabilizes the metal by inducing a sort of Peierls instability to a spin density wave (SDW) phase. As the field is varied, the SDW wave vector adjusts itself to ensure the Peierls condition that the Fermi level lies in the middle of one of the SDW Landau gaps. The key idea of the QNM is that the longitudinal component Q_x of the SDW nesting vector must be quantized according to $Q_x=2k_F+NG$, where $G=ebH/hc$ is the magnetic wave vector, b is the interchain distance and H is the magnetic field.

However, the $(TMTSF)_2ClO_4$ salt, which is much more widely studied since it undergoes the FISDW transitions at ambient pressure, has shown deviations from the theoretical predictions of the QNM.[13–20] In the high field regime ($H>18$ T) a nearly field independent second order transition takes place at 5.5 K from the metallic state to a SDW state. By decreasing the temperature, this transition is followed by a first order SDW-SDW transition at 3.5 K. The nature of these high field SDW states is enigmatic, in particular, the labeling of these subphases by a definite quantum number N is by no means obvious.

It has been proposed that the origin of the puzzling behavior of the $(TMTSF)_2ClO_4$ is due to the ClO_4^- anion ordering transition along the **b** direction perpendicular to the chains.[21–25] This transition takes place at a temperature $T_{AO}\sim 24$ K. For the slowly cooled (relaxed) ClO_4 salt, the anion ordering produces a periodic potential at a wave vector $(0,\pi/b,0)$. This doubles the unit cell in the **b** direction and opens a gap that causes neighboring chains to become inequivalent. Due to this gap, the original two-sheet Fermi

surface is split into four open sheets of Fermi surfaces. Obviously, the simplest Fermi surface model used in the standard version of QNM cannot apply anymore.

In this paper, we study the effect of the anion ordering on the high FISDW phases of $(TMTSF)_2ClO_4$. We extend discussions on the results we shortly presented in our previous paper[26] and address issues not considered in it. In the next section, we give a brief summary of the main experimental and theoretical results on $(TMTSF)_2ClO_4$. We will distinguish, in the theoretical review, two classes of models: those considering that the anion potential V is small and may then be treated as a perturbation and those assuming that V is too large, which prevents a perturbative treatment. In Sec. III, we analyze one of the two crucial points which make the originality of our work namely the competition between a single wave vector SDW phase and an original SDW phase induced by two nesting processes. The latter do not compete but on the contrary cooperate to stabilize this phase. We give the instability criterion for each SDW phase. The second crucial point of our model concerns the renormalization effects induced by low dimensional fluctuations on the electron-electron scattering strengths. We show, in Sec. IV, that these effects are different for different SDW phases, in particular for large V. To derive the complete phase diagram, we study in Sec. V, based on a Ginzburg-Landau expansion of the free energy, the relative stability of the different phases. The results are presented in Sec. VI where we consider the effects of some key parameters on the phase diagram. We show that the obtained results can explain consistently recent experimental data. Section VII is devoted to the concluding remarks.

II. OVERVIEW

A. Experimental results

The temperature-field phase diagram of the relaxed $(TMTSF)_2ClO_4$ was first obtained, at ambient pressure, by Naughton *et al.*[13] The authors found an unexpected feature: in the high magnetic field regime ($H>27$ T), the FISDW phase is destroyed and a reentrant metallic state appears (dotted line in Fig. 1). However, Yu *et al.* have reported the presence of a controversial insulating state above 27 T.[14]

Furthermore, the pressure dependence of the temperature-field phase diagram of $(TMTSF)_2PF_6$ and $(TMTSF)_2ClO_4$ was studied by Kang *et al.*[15] They found that the notable difference between the two compounds is the reentrant behavior followed by the transition to a very high field insulating phase in the case of the $(TMTSF)_2ClO_4$.

McKernan *et al.*[16] have established a phase diagram which is substantially different from previous results. They found that the low-field cascade of FISDW transitions is observed up to 8 T. As the field increases, the metal-SDW second order transition temperature continues to increase smoothly and saturates at 5.5 K above 15 T. On cooling from the metallic state, in the range from 23 T to 27 T, a first order transition occurs inside the original SDW phase with a maximum transition temperature of 3.5 K. The new transition line strongly decreases with increasing field and vanishes at 28 T. The 5.5 K and the 3.5 K phase boundaries do not show oscillations to better than 0.3 K.

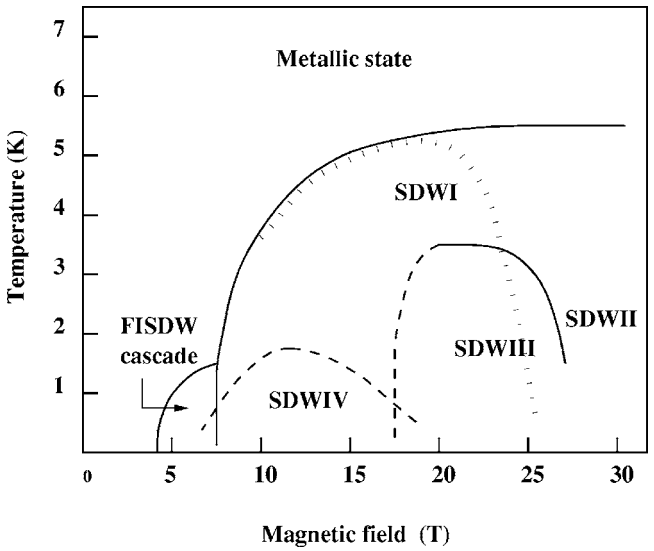

FIG. 1. Temperature-field phase diagram of $(TMTSF)_2ClO_4$. Solid lines are the transition boundaries obtained by McKernan *et al.* (Ref. 16), dashed ones are the results of Chung *et al.* (Ref. 20), while the dotted line is the high field phase boundary obtained by Naughton *et al.* (Ref. 13).

The substantial difference between the phase diagram of McKernan *et al.* and earlier ones are the presence of two distinct transitions in the region from 23 T to 27 T and the absence of any reentrant line. The latter may be obtained by crudely joining the 5.5 K and the 3.5 K lines (Fig. 1).

More recently, Moser *et al.*[19] have carried out magnetoresistance measurements up to 23 T and gave evidence for a crossover line between 17 T and 19 T, which appears as an extension of the 3.5 K phase boundary of McKernan *et al.* Such extension has been confirmed by Chung *et al.*[20] who concluded, based on magnetoresistance studies between 8 and 20 T, that the phase diagram shows more than two different subphases inside the main FISDW phase of the ClO_4 salt.

Figure 1 presents a generic temperature-magnetic field phase diagram where we summarize the different experimental results cited above. In this "arborescent" phase diagram there are so many subphases that it is not evident how to label them with definite quantum indexes. However, Hall effect measurements may reveal some key issues about the relationship between these different phases. Indeed, at 0.5 K, a stable quantum Hall-semimetal phase corresponding to $N=1$ plateau was observed from 7.5 to 27 T.[13,15,16] This plateau is somewhat spoiled above 15 T and shows, at high temperatures, besides oscillations, a slight accident at 17 T, which disappear above 3 K.[19] At 0.5 K, the very high field insulating state (SDWII phase in Fig. 1) is characterized by a nonquantized Hall resistance,[13,15,16] which is reminiscent of a $N=0$ SDW phase. It seems, therefore, that the subphases SDWIII and SDWIV may be indexed with $N=1$ while the SDWII may correspond to the $N=0$ phase. Since N cannot change unless a first order transition line is crossed, the SDWI subphase should also be associated to the $N=0$ state

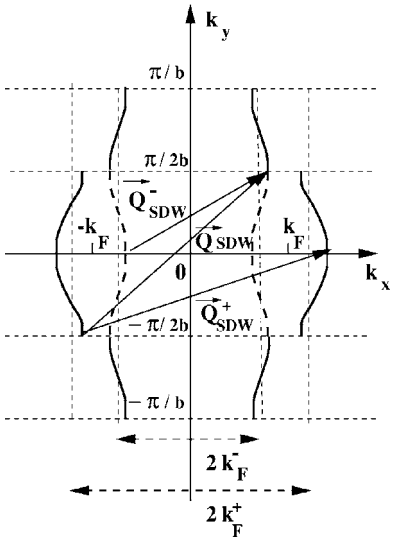

FIG. 2. Schematic Fermi surfaces of $(TMTSF)_2ClO_4$ under anion ordering. The dashed curves represent the reduced Fermi surface into the minizone $-\pi/2b \leqslant k_y \leqslant \pi/2b$. The SDW nesting vectors are $\vec{Q}_{SDW}=(2k_F,\pi/b)$, $\vec{Q}^{-}_{SDW}=(2k^{-}_F,\pi/2b)$ and $\vec{Q}^{+}_{SDW}=(2k^{+}_F,\pi/2b)$. k^{+}_F and k^{-}_F are the Fermi points of the four-sheet Fermi surface as defined in Refs. 28, 32, and 33.

as there is no transition boundary between this phase and the SDWII one.

Many authors attempted to analyze the complex behavior of the $(TMTSF)_2ClO_4$ phase diagram. In the following, we give a brief summary of the theoretical studies.

B. Theoretical aspects

In quasi-1D systems, the Fermi surface consists of two slightly warped open sheets. The electron dispersion relation is then approximated by:

$$\epsilon(\vec{k}) = v_F(|k_x| - k_F) - 2t_b \cos k_y b - 2t'_b \cos 2k_y b,$$

where k_x and k_y are the electron momenta, respectively, along and across the chains, v_F is the Fermi velocity and k_F is the Fermi point. t_b (t'_b) is the effective hopping integral to the first(second)-nearest neighbor. Due to the imperfect nesting parameter t'_b, $\vec{Q}_{SDW}=(2k_F,\pi/b)$ is not a perfect nesting vector for the band structure.

In the presence of the anion ordering, which introduces a periodic potential $V(y)=V\cos(\pi/b)y$, the band structure splits into two bands:[27]

$$\epsilon(\vec{k}) = v_F(|k| - k_F) \pm \sqrt{4t_b^2 \cos^2 k_\perp b + V^2} - 2t'_b \cos 2k_\perp b. \tag{1}$$

Equation (1) gives rise to two pairs of Fermi surfaces separated by a gap (Fig. 2). It should be noted that the anion gap does not break the nesting properties of the original Fermi surface since the two sheets are still related to each other through $\vec{Q}_{SDW}$ (Fig. 2).

Depending on the value of the V/t_b ratio, theoretical models may be classified into two groups: (i) small V models where V is supposed to be of the order of T_{AO} and the effects of the anion potential are studied within a perturbative treatment; (ii) large V models, where V may be of the order of t_b and is then considered nonperturbatively.

1. Small V models

Based on Landau's theory of second order transitions, these models suppose that V is of the order of $1.78T_{AO} \sim 50$ K, which is much smaller than $t_b \sim 200$ K. Considering V as a perturbation, Lebed and Bak[22] have found that the high field SDW transition line shows rapid oscillations and a reentrance of the metallic state. The SDW nesting vector used by the authors is $\vec{Q}_{SDW}$.

Osada *et al.*,[23] have also studied perturbatively the effect of the anion ordering on the high field phase diagram of $(TMTSF)_2ClO_4$. By calculating the noninteracting spin susceptibility $\chi_0(\vec{q})$, they have shown that the anion gap has no effect on the odd-N states for which $\chi_0(\vec{q})$ shows peaks at $q_x=2k_F+NG$ as in conventional FISDW phases. However, even-N states are found to be strongly suppressed. The corresponding peaks appear at $q_x=2k_F+NG\pm 2\delta/v_F$, where $\delta = VJ_0(4t_b/\omega_c)$, $\omega_c=v_FG$ is the magnetic energy and J_0 is the Bessel function. The authors have ascribed the reentrance of the metallic state, obtained by Naughton *et al.*,[13] to the suppression of the $N=0$ phase. They have also proposed that the very high field insulating state is the $N=0$ phase, which is expected to have an oscillating behavior. The predicted oscillations disagree with experiments, which have not given evidence of any oscillating phase boundary in the high field states.[13,15] Furthermore, the small V models[22,23,25] fail to explain the recently obtained experimental results, in particular, the presence of the first-order transition line at 3.5 K.[16,19,20] This failure has been thought to be due to the perturbation theory used to deal with the anion gap V.[28] Therefore, nonperturbative models have been proposed.

2. Large V models

Kishigi *et al.* have calculated the normal state susceptibility $\chi_0(\vec{q})$ for different values of V.[28–30] They showed that if $V \ll t_b$, the maximum of $\chi_0(\vec{q})$ is at $\vec{Q}_{SDW}$ as found by Osada *et al.* However, if $V \sim t_b$, the peaks of $\chi_0(\vec{q})$ correspond to $\vec{Q}^{\pm}_{SDW}=(2k^{\pm}_F,\pi/2b)$, where $k^{\pm}_F$ are the Fermi points of the four-sheet Fermi surfaces (Fig. 2). The authors have also studied, using a self-consistent numerical calculations, the ordered state below the transition temperature in the presence of a magnetic field.[30,31] They found that the system undergoes a second order transition from the metallic state to a FISDW state for which the nesting vector is $\vec{Q}_{SDW}=(2k_F,\pi/b)$. Hence, for this state, both pairs of the Fermi surfaces are gapped. Furthermore, they obtained a first order transition line from the previous SDW state to an other SDW phase where the nesting vector is $\vec{Q}^{-}_{SDW}=(2k^{-}_F,\pi/2b)$. In this case, only one pair of the Fermi surfaces disappears. This phase is, however, destabilized at low temperature and a second order transition takes place, giving rise to a SDW state originating from two coexisting nesting vectors: $\vec{Q}^{+}_{SDW}=(2k^{+}_F,\pi/2b)$ and $\vec{Q}^{-}_{SDW}=(2k^{-}_F,\pi/2b)$.

Apart from this last state, the authors argued that their results are similar to the experimental ones reported by McKernan *et al.* The transition lines corresponding to the phase with $\vec{Q}_{SDW}$ and that associated to $\vec{Q}^{-}_{SDW}$ were, respectively, ascribed to the 5.5 K and the 3.5 K boundary phases.

McKernan *et al.* have, already, suggested a scenario of separate SDW transitions taking place successively on each pair of the Fermi surfaces. They have also proposed the coexistence of two nesting processes to explain the formation of the inner phase, resulting from the first order transition at 3.5 K.

Nevertheless, the coexisting state obtained by Kishigi[31] does not correspond to the inner phase appearing at 3.5 K. The former is induced by a second order transition while the latter is due to a first order one. On the other hand, besides its large quantitative disagreement with experiments, the proposed phase diagram of Kishigi does not account for the behavior of the inner phase in the low field regime.[19,20] Moreover, it is not obvious, within this model, how to label the different subphases by definite quantum indexes.

More recently, Sengupta and Dupuis[32] have studied the effect of anion ordering on the SDW state in the absence of a magnetic field. They derived a generalized Stoner criterion that yields to three kinds of SDW instabilities with three possible nesting vectors: an interband nesting $\vec{Q}_{int}$ and two intraband nestings $\vec{Q}_{+}$ and $\vec{Q}_{-}$. These vectors are identical to those proposed by Kishigi *et al.* and correspond respectively to $\vec{Q}_{SDW}$, $\vec{Q}^{-}_{SDW}$, and $\vec{Q}^{+}_{SDW}$. The authors have shown that the interband SDW instability is destroyed as V increases, whereas the intraband SDW instability is furthered. From the Ginzburg-Landau expansion of the free energy, the authors found that if V is of the order of t_b, two successive instabilities are possible by decreasing the temperature. The first one, which is a second-order metal-SDW transition, opens a gap on only one band of the Fermi surface while the other band remains gapless. At the second transition, which is also of second order, the whole Fermi surface becomes gapped and a coexisting state of two SDW intraband pairings is formed. These successive transitions have been associated to that obtained by McKernan *et al.* However, the latter are separated by a first order transition line and not by a second one as suggested by Sengupta and Dupuis.

Similar results have been obtained by Zanchi and Bjeliš[33] who considered, within a matrix random phase approximation (RPA), the intraband and the interband SDW instabilities in ClO_4 salt in the absence of a magnetic field. They found that, the intraband SDW states, denoted $SDW_{\pm}$, are stable at high values of V. These states are separated from the interband SDW one (SDW_0), which appears at low V values, by a valley corresponding to the intermediate V values, where the metallic state may persist.

Radić *et al.*[34] have studied, within the matrix RPA developed in Ref. 33, the effect of a magnetic field on these different SDW states. The authors found, as proposed by Osada *et al.*,[23] that odd-N-FISDW phases originate from interband processes while even-N phases are due to intraband processes. The anion splitting has then no effect on the odd-N phases. By taking $V \sim 0.8t_b$, the authors have reproduced the rapid oscillations periodicity of 260 T observed experimentally.[18,20]

The temperature-field phase diagram derived by Radić *et al.* shows the presence of a first order transition from the low field odd N SDW phases (SDW_0) to the high field intraband phase ($SDW_{\pm}$). The latter is characterized by an oscillating transition line which tends to saturate with increasing field. These oscillations are not consistent with experimental results showing that any phase boundary oscillations should be certainly less than 0.3 K.[16] Furthermore, the phase diagram of Radić *et al.* does not include the inner phase obtained experimentally. The authors argued that such phase may be obtained taking into account higher harmonic terms in the dispersion relation [Eq. (1)] as done in Ref. 32. This phase will then be the result of two successive transition scenarios as proposed by many authors.[16,31,32]

However, the assumption of two successive transitions cannot agree with the experimental data. Let us consider, as proposed by Radić *et al.*, that the first transition takes place at $T_c(SDW_-)$ where only one band is gapped. Then, a second transition occurs at $T_c(SDW_+)$ and now a gap opens on the whole Fermi surface. This scenario means that only half of the density of states (DOS) is involved during the first transition while the whole DOS is taken into account during the second one. Considering the Fermi energy $E_F = 3000$ K and $T_c(SDW)_= 5.5$ K gives a ratio of 5.5/3000 for $T_c(SDW)_-/T_c(SDW)_+$ whereas the experimental data yields to a ratio of 5.5/3.5. The occurrence of two successive transitions is then in disagreement with experiments

Moreover, as we will show in the next section, the indexation with definite quantum numbers N of the different FISDW phases obtained in Ref. 34 cannot correspond to that obtained by Hall effect measurements. Given all these theories, one may conclude that neither small V models nor large V ones discussed above can account, in a consistent manner, for the whole experimental results.

We have proposed in Ref. 26 a model where V is supposed to be small compared to t_b. Our model introduces original concepts which have been overlooked in previous works. Since there remains some controversy about the V value, we will discuss in the following the arguments in favor of a weak value ($V \ll t_b$) and those which support a rather strong value ($V \sim t_b$).

C. Discussion about the anion potential value

1. Quantum chemistry calculations

Quantum chemistry calculations have been performed to study the band structure of the Bechgaard salts, in particular the $(TMTSF)_2ClO_4$ compound. The agreement between these calculations and the experimental data can be considered as very good.[1] However, the determination of the effect of anion ordering on the electron band structure in ClO_4 salt is much more difficult. Because of the symmetry of the anion ordering in this specific salt, its effect on the electron spectrum involves delicate balance between self-consistent potentials created by tiny transverse displacements of the ClO_4 anions. At the present time, it is hopeless to try to determine the anion gap V from such quantum chemistry calculations.[35] Le Péleven *et al.*,[36] whose work has been peculiarly quoted

by many authors as a proof of a large V value,[32–34] do not even propose a value for V and argued that the quantitative evaluation of the anion potential is *out of reach* of their method. We are, then, led to the conclusion that no quantum chemistry calculations provide any proof of a large V value, contrary to some claims.[33,34]

2. Analysis of the angular dependence of the magnetoresistance

The anomalous giant magnetoresistance of the Bechgaard salts is probably one of the less understood and the most controversial phenomenon observed in low dimensional organic conductors.[37] However, several authors have proposed to determine the Fermi surface geometry of some organic conductors from an analysis of the angular dependence of the magnetoresistance (ADM). Such determination cannot be done without ambiguities as proved by many authors.[38,39] Given the non-Fermi liquid behavior recently observed and discussed in the Bechgaard salts,[40] one should be cautious about a precise determination of V based on the ADM measurements. In spite of these peculiarities, there have been some attempts to interpret such data.

Yoshino *et al.*[41] have observed an anomaly of the ADM in the relaxed ClO_4 salt. From a simple semiclassical model, the authors suggested that V is of the order of $0.08t_a$, where $t_a \sim 10t_b$ is the hopping parameter along the most conducting axis. Nevertheless, they concluded themselves that it is hard to assume such a large value and that more detailed analysis is necessary.

Osada *et al.*[42] have also measured the ADM in ClO_4 salt. They found that the V value cannot be estimated from their data due to the presence of a two pairs of sheetlike Fermi surfaces. Uji *et al.*[43] have proposed, from the same kind of experimental procedure, using also a semiclassical model the value of $V \sim 50$ K.

It should be stressed that, the experimental value of V proposed by Yoshino *et al.*[41] was substantially the key argument for the large V models[31,33] Nevertheless, this value has been renewed recently by the same group[44] who found a much smaller value of V which is estimated to $0.023t_a$. This value corresponds to the small V regime in the theoretical phase diagrams obtained in Refs. 32 and 33.

More recently Lebed *et al.* have proposed that the angular magnetoresistance oscillations in quasi-one-dimensional conductors are due to 1D-2D dimensional crossovers which take place at some commensurate directions of the magnetic field.[45] The authors suggested to make use of this effect to determine the band parameters of quasi-1D conductors such as the anisotropy ratio t_a/t_b and the anion gap V. In Ref. 46, Ha *et al.* reported angle-dependent magnetoresistance measurements on the $(TMTSF)_2ClO_4$. The analysis of the magnetoresistance oscillations based on the model proposed in Refs. 45 gives rise to a value of $V=0.2t_b$ for the anion potential. The authors argued that such method is the most accurate way to determine the anion gap. Therefore, ADM measurements clearly support the idea that V is much smaller than the interchain hopping parameter t_b.

3. Theoretical estimations of the phase diagram

In this paragraph, we will discuss the results of the theoretical models, presented in Sec. II, which suggest a strong V value.

In their theoretical phase diagram, Zanchi and Bjeliš[33] have fixed a constraint on the possible values of V which should be in the range of $0.1t_b$ to $1.6t_b$. Therefore, a small value of V is not necessary excluded within this work. On the other hand, the experimental data on ClO_4 salt, prepared with different cooling rates show that the metallic state is rapidly destroyed when the anion gap is reduced.[47,48] One may, then, conclude that the real value of V is much closer to the $0.1t_b$ limit than to the upper one. Indeed, a large domain, in which the metallic state persists, separate the SDW state appearing at small V (SDW_0 state) from those corresponding to the large V ($SDW_\pm$ state) (Fig. 3 of Ref. 33).

Sengupta and Dupuis,[32] suggested that V should be of the order of t_b to explain the successive transitions found by McKernan *et al.*[16] However, for a such value, the ground state, at zero field, is magnetic, which is in disagreement with experiments suggesting a superconducting state. On the other hand, this model suppose a sizeable departure from perfect nesting, for large V, which cannot account for the FISDW cascade at low field.

Furthermore, the successive transition scenario is, as we have discussed above, in quantitative disagreement with the experimental data. Kishigi *et al.*[28,29,31] argued that V should be of the order of t_b, since, in this case, the metal-SDW critical temperature becomes field independent as found experimentally. However, this conclusion is not justified since we have obtained a field independent boundary line assuming a small V value.[26]

4. Thermodynamics of the anion ordering

A simple energetic argument shows that V cannot be larger than the critical temperature of the anion ordering T_{AO}. Indeed, the typical energy involved in the phenomenon of anion ordering cannot be very different from $k_B T_{AO}$. Since the gap V is the result of the perturbation induced by anion ordering, obviously, V cannot be larger than the energy causing this perturbation. Within the Landau's theory of second order transitions, V is supposed to be of the order of $1.78T_{AO} \sim 50$ K.

5. Structural studies of the anion ordering

By joint measurements of x ray diffusion, NMR and transport properties, the Orsay group on structural studies of organic conductors has performed detailed studies dealing with the structure of the Bechgaard salts, in particular the ClO_4 salt. They studied the formation of domains, in which the anions are ordered when the cooling rate through T_{AO} is varied.[47,48] From these experiments, the authors have given an estimate of $V \sim 12$ K, which is much smaller than t_b.

6. Departure from perfect nesting

The departure from perfect nesting of the Fermi surface is a crucial parameter for many properties of $(TMTSF)_2ClO_4$, particularly for the well known cascade of FISDW phases. In the case of small V, the low field phase diagram ($H < 10$ T) is extremely well accounted for, if the departure from perfect nesting is $t_b' \sim 10$ K. However, if $V \sim t_b$, this is no longer the case.[33] In that limit, the departure from perfect

nesting is not given by t_b' but essentially by V.[29] A value of $V \sim t_b$ leads to a departure from perfect nesting ~50 K i.e., five times larger than the value necessary to interpret the quantum cascade.

7. Quantum Hall effect

The Hall plateaus measured in the regime between 3 T and 10 T were labeled by low values of quantum numbers $(N=4,3,2,1)$.[13,16] The calculated numbers N in Ref. 29, where the authors assumed that $V \sim t_b$, are quite large. As proved by Hasegawa *et al.*,[29] one should expect large quantum numbers for large V: $N \sim 2V/\omega_c$, which is strongly incompatible with experiments.

This discrepancy is due to the fact that the model of Ref. 29 brings into play a large deviation from perfect nesting which is of the order of V. Hasegawa *et al.*[29] assumed that the coexistence of multiple order parameters might explain such discrepancy. However, Yakovenko has shown that, in the case of multiple order parameters, the quantum plateau should simply be given by the largest one.[49] Therefore, the succession of small quantum numbers observed experimentally cannot be recovered within the model of Ref. 29 in the limit of large V.

Nevertheless, Radić *et al.* claimed that their model suggesting a large V value can account for the quantum Hall effect. They estimated the departure from perfect nesting to be

$$\Delta E = \sqrt{V^2 + 2t_b^2} - (\sqrt{V^2 + 4t_b^2} + V)/2.$$

This equation gives $\Delta E \sim t_b/10$ for $V \sim t_b$. The obtained quantum numbers $N \sim \Delta E/\omega_c$ take the values between 3 and 1 for magnetic fields between 10 T and 30 T.

However, these quantum numbers, though small, cannot explain the Hall effect measurements where the $N=1$ plateau has been observed at $H=10$ T and not 30 T as reported in Ref. 34. Moreover, Radić *et al.* argued that the SDW_+ phase and the SDW_- one are ascribed to *even* quantum numbers while the SDW_0 state corresponds to an *odd-N*. The authors have suggested that the 5.5 K and the 3.5 K lines, obtained experimentally, may be associated respectively to the SDW_- and the SDW_+ phases if these two phases are actually separated. Therefore, according to Radić *et al.*, the original phase (SDW_-) and the inner one (SDW_+) will be indexed by the *same even-number N*, while experiments suggest different quantum numbers for the two phases.

Recently, Matsunaga *et al.*[50] have carried out magnetoresistance measurements in the $(TMTSF)_2ClO_4$ for various cooling rates. The authors come down to the conclusion that the inner phase and the insulating high field state correspond to *different FISDW states*. Furthermore, it has been reported from experimental studies[13,16] that the inner phase shows a $N=1$ quantum Hall plateau, starting from 8 T, rather than an even-N one as supposed by Radić *et al.*[34]

From all these remarks, we can conclude that there is no direct unambiguous determination of V. Moreover, the assumption according to which $V \sim t_b$ is not justified and makes very difficult the interpretation of the quantum cascade of FISDW phases and the quantized Hall effect. Such large V value seems to be difficult to accept.

In the following, we present our model where we consider a small anion gap V. We will not discuss in this paper the rapid oscillations observed in the magnetoresistance measurements of the $(TMTSF)_2ClO_4$. This will be the subject of a forthcoming work.

III. INSTABILITY CRITERIA

In the absence of anion ordering, the quasi-1D electron spectrum is given by Eq. (1). We neglect in this equation, and hereafter, the dispersion along the least conducting axis (z axis), which is not relevant for our model.

When a magnetic field is applied along the z direction, and in the Landau gauge $\mathbf{A}=(0,Hx,0)$, the noninteracting Hamiltonian takes the form

$$H_{eff}^0 = v_F\left[\left|-i\frac{\partial}{\partial x}\right| - k_F\right] - 2t_b\cos\left[-ib\frac{\partial}{\partial y} + ebHx\right] - 2t_b'\cos\left[-2ib\frac{\partial}{\partial y} + 2ebHx\right].$$

In the Wannier representation, the eigenfunctions of H_{eff}^0 can be written as

$$\psi_{K_x,l}(\vec{r}) = \frac{b}{2\pi}\int_0^{2\pi/b} dK_y \exp(-ilK_y b)\langle\vec{r}|F_{\vec{k}}^0\rangle,$$

where $\vec{K}=(K_x,K_y,K_z)$ is the quantum numbers. The integer l is used instead of K_y and $|F_{\vec{k}}^0\rangle$ is the eigenstate of H_{eff}^0 given by[23]

$$\langle\vec{r}|F_{\vec{k}}^0\rangle = \frac{1}{\Omega^{1/2}}\exp\left[i\vec{K}\cdot\vec{r} + i\,\mathrm{sgn}(K_x)\left\{\frac{2t_b}{v_F G}\sin(Gx + bK_y) + \frac{t_b'}{v_F G}\sin(2Gx + 2bK_y)\right\}\right],$$

where Ω is the system volume and $G=eHb$ is the magnetic wave vector. We use the units $\hbar=k_b=c=1$.

Due to the anion ordering, which gives rise to the superlattice potential $V(y)=V\cos\pi/by$, the Brillouin zone is halved in the k_y axis. We suppose that the anion gap V is small enough to be considered as a perturbation. In the $\{|\psi_{K_x,l}\rangle\}$ basis, the matrix elements of the anion potential $V(y)$, are given by[22,51]

$$\langle\psi_{2\pi n/L,l}|V|\psi_{2\pi n'/L,l'}\rangle = V(-1)^l J_{l'-l}\left(\frac{4t_b}{v_F G}\right)\times\delta\left(n - n' + \frac{LG(l-l')}{2\pi}\right). \quad (2)$$

L is the length of the sample along the chain direction and J is the Bessel function.

Up to the first order of perturbation, the diagonal term with $l=l'$ in Eq. (2) splits the energy spectrum of the total Hamiltonian into two linearized subbands E^A and E^B given by (Fig. 3)

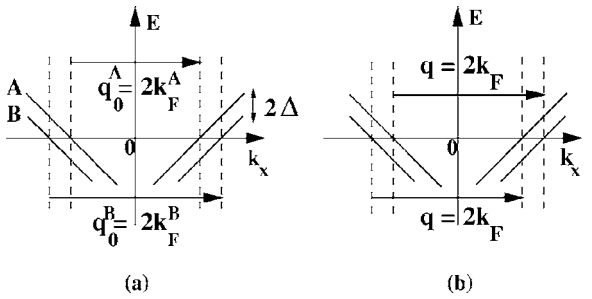

FIG. 3. Band structure of quasi-1D electron system in the presence of anion ordering. q_0^A and q_0^B are intraband nesting vectors respectively in the A band and the B band while q corresponds to the interband nesting vector.

$$E_{\vec{k}}^m = v_F(|k_x| - k_F^m),$$

where $m=A,B$ is the band index and k_F^m are the Fermi momenta written as $k_F^A=k_F-\Delta/v_F$ and $k_F^B=k_F+\Delta/v_F$. Here Δ is the effective anion gap given by

$$\Delta = VJ_0\left(\frac{4t_b}{v_F G}\right). \tag{3}$$

Due to the splitting of the band structure into two subbands, three nesting processes are made possible: two intraband nestings involving two wave vectors: $q_A^0=2k_F^A$ and $q_B^0=2k_F^B$ and an interband nesting process with a single nesting vector $q=2k_F$, as in the case of a single band structure (Fig. 3).

In a Fermi liquid approach, the instability of the metallic phase is discussed by writing the Stoner criterion, which involves the noninteracting spin susceptibilities $\chi_0(\vec{q})$. Osada *et al.*[23] have shown that $\chi_0(\vec{q})$ may be separated into four terms corresponding to four combinations of the electron-hole pairing in two subbands: two intraband pairings, where the electron and the hole belong to the same band, and the two interband ones for which the particles are on different bands. The authors have found that the intraband terms show peaks at $q_x=2k_F^m+2MG$, where M is an integer, whereas the interband terms have peaks at $q_x=2k_F+(2M+1)G$. Therefore, the formation of a SDW phase with an *even* value of the quantum number is associated to the divergence of the *intraband* susceptibilities while that ascribed to a SDW state with an *odd* quantum number corresponds to the divergence of the *interband* susceptibilities. It is worth noting that the FISDW states appearing in the high field regime correspond to the smallest quantum numbers. Experimentally, the SDW phases associated to $N=3$ and $N=2$ are observed in the low field regime ($H<10$ T). In the following, we shall focus on the $N=0$ and $N=1$ FISDW states since we are interested in the high magnetic field regime.

Unlike Ref. 23, we take into account the interaction between electrons within the following Hamiltonian:

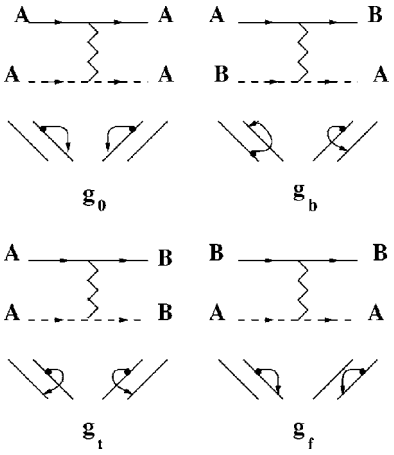

FIG. 4. Different forward scattering processes generated in the presence of two bands. Solid (dashed) lines represent right (left) moving electrons.

$$\begin{aligned}
H_{int} = {} & g_0 \sum_m \sum_\sigma \int d\vec{r}\, \psi^\dagger_{m\alpha\sigma}(\vec{r})\psi^\dagger_{m\bar{\alpha}\bar{\sigma}}(\vec{r})\psi_{m\bar{\alpha}\bar{\sigma}}(\vec{r})\psi_{m\alpha\sigma}(\vec{r}) \\
& + g_f \sum_m \sum_\sigma \int d\vec{r}\, \psi^\dagger_{m\alpha\sigma}(\vec{r})\psi^\dagger_{\bar{m}\bar{\alpha}\bar{\sigma}}(\vec{r})\psi_{\bar{m}\bar{\alpha}\bar{\sigma}}(\vec{r})\psi_{m\alpha\sigma}(\vec{r}) \\
& + g_t \sum_m \sum_\sigma \int d\vec{r}\, \psi^\dagger_{\bar{m}\alpha\sigma}(\vec{r})\psi^\dagger_{\bar{m}\bar{\alpha}\bar{\sigma}}(\vec{r})\psi_{m\bar{\alpha}\bar{\sigma}}(\vec{r})\psi_{m\alpha\sigma}(\vec{r}) \\
& + g_b \sum_m \sum_\sigma \int d\vec{r}\, \psi^\dagger_{\bar{m}\alpha\sigma}(\vec{r})\psi^\dagger_{m\bar{\alpha}\bar{\sigma}}(\vec{r})\psi_{\bar{m}\bar{\alpha}\bar{\sigma}}(\vec{r})\psi_{m\alpha\sigma}(\vec{r}).
\end{aligned}$$

$\psi_{m\alpha\sigma}(\vec{r})$ denotes a fermionic operator for right ($\alpha=1$) or left ($\alpha=2$) moving particles on the band labeled m ($m=A,B$) and with a spin σ. m and $\bar{m}$ (α and $\bar{\alpha}$) denote different bands (branches) and $\bar{\sigma}=-\sigma$.

The coupling constants g_μ, ($\mu=0,f,t,b$), depicted in Fig. 4, correspond to the forward scattering term g_2 within the *g-ology* model.[52] We have neglected in the interacting part of the Hamiltonian the backward scattering (g_1), which is irrelevant in the mean field theory (MFT) of FISDW phases. We have not, also, included the umklapp scattering (g_3) since it does not play a central role in our model.

In the mean field (MF) approximation, H_{int} reads as

$$\begin{aligned}
H_{int}^{MF} = {} & -g_0 \sum_m \sum_\sigma \int d\vec{r} \langle \psi_{m\bar{\alpha}\bar{\sigma}}\psi^\dagger_{m\alpha\sigma}(\vec{r})\rangle \psi_{m\alpha\sigma}(\vec{r})\psi^\dagger_{m\bar{\alpha}\bar{\sigma}}(\vec{r}) \\
& - g_f \sum_m \sum_\sigma \int d\vec{r} \langle \psi_{\bar{m}\bar{\alpha}\bar{\sigma}}\psi^\dagger_{m\alpha\sigma}(\vec{r})\rangle \psi_{m\alpha\sigma}(\vec{r})\psi^\dagger_{\bar{m}\bar{\alpha}\bar{\sigma}}(\vec{r}) \\
& - g_t \sum_m \sum_\sigma \int d\vec{r} \langle \psi_{m\bar{\alpha}\bar{\sigma}}\psi^\dagger_{\bar{m}\alpha\sigma}(\vec{r})\rangle \psi_{m\alpha\sigma}(\vec{r})\psi^\dagger_{\bar{m}\bar{\alpha}\bar{\sigma}}(\vec{r}) \\
& - g_b \sum_m \sum_\sigma \int d\vec{r} \langle \psi_{\bar{m}\bar{\alpha}\bar{\sigma}}\psi^\dagger_{\bar{m}\alpha\sigma}(\vec{r})\rangle \psi_{m\alpha\sigma}(\vec{r})\psi^\dagger_{m\bar{\alpha}\bar{\sigma}}(\vec{r}).
\end{aligned} \tag{4}$$

As we have discussed above, the stability of the $N=0$ phase

is due to the intraband processes. Therefore, only the g_0 and g_b terms in H_{int}^{MF} are relevant for the $N=0$ phase, since the annihilated particle and hole are on the same band. However, for the $N=1$ phase, which is induced by interband processes, the g_t and g_f terms, where the diffused hole and particle belong to different bands, are the determining parts of the Hamiltonian.

Let us focus on the $N=0$ phase for which one should define two order parameters due to the presence of two different intraband nesting vectors q_A^0 and q_B^0. We denote by Δ_A^0 and Δ_B^0 the order parameters, respectively, for the A band and the B band:

$$\Delta_m^0(\vec{r}) = -g_0\langle\psi_{m2\bar{\sigma}}(\vec{r})\psi_{m1\sigma}^{\dagger}(\vec{r})\rangle\exp^{i\vec{Q}_m^0\cdot\vec{r}},$$

where $\vec{Q}_m^0=(2k_F^m, q_\perp^0)$ and $q_\perp^0$ is the transverse component of $\vec{Q}_m^0$.

It should be noted that for a phase with an even N quantum number the order parameter in the m band takes the form

$$\Delta_m^N(\vec{r}) = -g_0\langle\psi_{m2\bar{\sigma}}(\vec{r})\psi_{m1\sigma}^{\dagger}(\vec{r})\rangle\exp^{i\vec{Q}_m^N\cdot\vec{r}},$$

where $\vec{Q}_m^N=(2k_F^m+NG, q_\perp^N)$.

The interacting part of the mean field Hamiltonian in the $N=0$ phase can, then, be written as

$$\begin{aligned}H_0^{MF} = &\sum_m\sum_\sigma\int d\vec{r}\{\Delta_m^0(\vec{r})\exp^{-i\vec{Q}_m^0\cdot\vec{r}}\,\psi_{m1\sigma}(\vec{r})\psi_{m2\bar{\sigma}}^{\dagger}(\vec{r})\\ &+[\Delta_m^0(\vec{r})]^*\exp^{i\vec{Q}_m^0\cdot\vec{r}}\,\psi_{m2\bar{\sigma}}(\vec{r})\psi_{m1\sigma}^{\dagger}(\vec{r})\}\\ &+\frac{g_b}{g_0}\sum_m\sum_\sigma\int d\vec{r}\{\Delta_{\bar{m}}^0(\vec{r})\exp^{-i\vec{Q}_{\bar{m}}^0\cdot\vec{r}}\,\psi_{m1\sigma}(\vec{r})\psi_{m2\bar{\sigma}}^{\dagger}(\vec{r})\\ &+[\Delta_m^0(\vec{r})]^*\exp^{i\vec{Q}_m^0\cdot\vec{r}}\,\psi_{\bar{m}2\bar{\sigma}}(\vec{r})\psi_{\bar{m}1\sigma}^{\dagger}(\vec{r})\}.\end{aligned}$$

We now use the formalism introduced in Refs. 8 and 53 and we define the following Green functions in the m band:

$$F_m^0(\bar{r},\bar{r}') = -\langle T_\tau[\psi_{m2\downarrow}(\bar{r})\psi_{m1\uparrow}^{\dagger}(\bar{r}')]\rangle\exp^{i\vec{Q}_m^0\cdot\vec{r}},$$

$$G_m^0(\bar{r},\bar{r}') = -\langle T_\tau[\psi_{m1\uparrow}(\bar{r})\psi_{m1\uparrow}^{\dagger}(\bar{r}')]\rangle,$$

where $\bar{r}=(\vec{r},\tau)$.

In the mixed representation,[8,53] and after taking the Fourier transforms with respect to time, the Gor'kov equations in the Landau gauge $\vec{A}=(0,Hx,0)$ for the m band reads as

$$\begin{aligned}&\left[i\omega_n+\mu_BH+iv_F\frac{d}{dx}+v_Fk_F^m-\epsilon_\perp\left(p-\frac{x}{x_0}\right)\right]G_m^0\\ &\quad+\left[(\Delta_m^0)^*+\frac{g_b}{g_0}(\Delta_{\bar{m}}^0)^*\exp\left(-i\frac{4\Delta}{v_F}x\right)\right]F_m^0=\delta(x-x'),\\ &\left[i\omega_n-\mu_BH-iv_F\frac{d}{dx}-v_Fk_F^m-\epsilon_\perp\left(p+q_\perp^0b-\frac{x}{x_0}\right)\right]F_m^0\\ &\quad+\left[\Delta_m^0+\frac{g_b}{g_0}\Delta_{\bar{m}}^0\exp\left(i\frac{4\Delta}{v_F}x\right)\right]G_m^0=0.\end{aligned}\tag{5}$$

In Eq. (5), ω_n are the Matsubara frequencies, Δ is the effective anion gap [Eq. (3)] and μ_BH is the Zeeman term. $\epsilon_\perp(k_y)$ is the dispersion relation in the **b** direction:

$$\epsilon_\perp(k_y) = -2t_b\cos k_yb - 2t_b'\cos 2k_yb.$$

We have set $x_0=1/G=1/eHb$, $p=k_yb$ and $q_\perp^0=\pi$ as shown within the QNM.

Equation (5) is said to be written in the mixed representation since it depends on the longitudinal component in the direct space (x) and the transverse one in the reciprocal space (p). Unlike the case of single band structure,[8,53] we have an additional term in Eq. (5) due to the presence of the g_b process and the anion gap.

We define as in Ref. 8

$$\begin{aligned}g_m^0(x,x') = G_m^0(x,x')\exp\Bigg[&-i\left(\frac{\mu_BH}{v_F}-k_F^m\right)(x-x')\\ &+\frac{i}{v_F}\int_{x'}^{x}\epsilon_\perp\left(p-\frac{u}{x_0}\right)du\Bigg],\end{aligned}$$

$$\begin{aligned}f_m^0(x,x') = F_m(x,x')\exp\Bigg[&i\left(\frac{\mu_BH}{v_F}-k_F^m\right)(x-x')-\frac{i}{v_F}\int_0^x\epsilon_\perp\\ &\times\left(p-\frac{u}{x_0}-q_\perp^0b\right)du-\frac{i}{v_F}\int_0^{x'}\epsilon_\perp\left(p-\frac{u}{x_0}\right)du\Bigg],\end{aligned}$$

$$\begin{aligned}\tilde{\Delta}_m(x,p) = [\Delta_m^0(x)]^*\exp\frac{i}{v_F}\Bigg[&\int_0^x\epsilon_\perp\left(p-\frac{u}{x_0}-q_\perp^0b\right)du\\ &+\int_0^x\epsilon_\perp\left(p-\frac{u}{x_0}\right)du\Bigg].\end{aligned}$$

Equation (5) then takes a simpler form:

$$\begin{aligned}&\left(i\omega_n+iv_F\frac{d}{dx}\right)g_m^0+\left[\tilde{\Delta}_m+\frac{g_b}{g_0}\tilde{\Delta}_{\bar{m}}\exp\left(-i\frac{4\Delta}{v_F}x\right)\right]f_m^0\\ &\quad=\delta(x-x'),\\ &\left(i\omega_n-iv_F\frac{d}{dx}\right)f_m^0+\left[\tilde{\Delta}_m^*+\frac{g_b}{g_0}\tilde{\Delta}_{\bar{m}}^*\exp\left(i\frac{4\Delta}{v_F}x\right)\right]g_m^0=0.\end{aligned}$$

We consider the Fourier expansion of $f_m^0(x,x')$ and $g_m^0(x,x')$. We denote by $f_j^{m(0)}(k,\omega_n)$ and $g_j^{m(0)}(k,\omega_n)$ the respective Fourier components which obey to[53]

$$\begin{aligned}&(i\omega_n-v_Fk)g_0^{m(0)}(k,\omega_n)\\ &\quad+\sum_j\left[\delta_j^m+\frac{g_b}{g_0}\delta_j^{\bar{m}}\exp\left(-i\frac{4\Delta}{v_F}x\right)\right]f_j^{m(0)}(k,\omega_n)=1,\\ &(i\omega_n+v_Fk)f_0^{m(0)}(k,\omega_n)\\ &\quad+\sum_j\left[(\delta_j^m)^*+\frac{g_b}{g_0}(\delta_j^{\bar{m}})^*\exp\left(i\frac{4\Delta}{v_F}x\right)\right]g_{-j}^{m(0)}(k,\omega_n)=0,\end{aligned}$$

where $\delta_n^m=I_n(q_\perp^0)\Delta_m^0$ and I_n are the well known coefficients defined in the QNM.[5]

The self-consistency condition reads as[8]

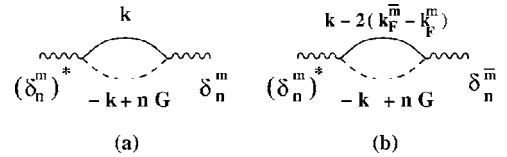

FIG. 5. Diagrammatic representation of the first term (a) and the second one (b) of the generalized Stoner criterion given by Eq. (7). $\delta_n^m = I_n \Delta_m^0$ $(m=A,B)$.

$$\Delta_m^0 = g_0 T \sum_{\omega_n} \langle F_m^0(x,x',p,\omega_n)\rangle_p, \tag{6}$$

where $\langle \ldots \rangle_p$ denotes the average over p. By replacing $F_m(x,x',p,\omega_n)$ with its corresponding expression using $f_j^{m(0)}(k,\omega_n)$, we deduce from Eq. (6) the following Stoner criterion for the $N=0$ phase:

$$\frac{1}{g_0} = \frac{1}{2}\chi_m^0(\vec{Q}_m^0,T) + \frac{1}{2}\frac{g_b}{g_0}\chi_m'\left(\frac{4\Delta}{v_F},T\right). \tag{7}$$

$\chi_m^0(\vec{Q}_m^0,T)$ is the bare susceptibility in the m band:

$$\chi_m^0(\vec{Q}_m^0,T) = \sum_n I_n^2(q_\perp^0)\chi_m^{1D}(q_m^0 - nG,T),$$

where $q_0^m = 2k_F^m$ is the longitudinal component of the nesting vector $\vec{Q}_m^0$. As defined in QNM, $\chi_m^{1D}(q_x)$ is the bare susceptibility of a one-dimensional system which has logarithmic divergence at quantized values $q_x = 2k_F^m + nG$:[4,5,9]

$$\chi_m^{1D}(q_x) = N(0)\left[\ln\left(\frac{2\gamma E_0}{\pi T}\right) + \Psi\left(\frac{1}{2}\right) - \mathrm{Re}\,\Psi\left(\frac{1}{2} + i\frac{v_F(q_x - 2k_F^m)}{4\pi T}\right)\right], \tag{8}$$

where Ψ is the digamma function, Re Ψ is its real part, $N(0)$ is the density of states and $\gamma \sim 1.783$ is the exponential of the Euler constant.

$\chi_m^0(q_0^m,T)$ describes the SDW instability, at the wave vector q_0^m, which opens a large gap at the Fermi level k_F^m of the m band and a much smaller one on the $\bar{m}$ band but outside of its Fermi level. However, χ_m' term correspond to the minority SDW component that forms on the m band outside the Fermi level and which is due to the SDW instability occurring on the $\bar{m}$ band. χ_m' is given by

$$\chi_m'\left(\frac{4\Delta}{v_F},T\right) = \sum_n I_n^2(q_\perp^0)\chi_m^{1D}(q_m^0 + 2(k_F^{\bar{m}} - k_F^m) - nG,T). \tag{9}$$

The χ_m' term does not exist in the standard Stoner criterion of FISDW derived in the case of a single band energy spectrum.[5] It should be stressed that Eq. (7) is a generalized Stoner criterion for the $N=0$ phase in the presence of the anion gap and under a magnetic field. Figure 5 shows the Feynman diagrams used to derive the spin susceptibilities χ_m^0 and χ_m'.

In Ref. 34, the authors asserted that, to derive the phase diagram of Ref. 26, we have applied the standard Stoner criterion used in the QNM. Actually, we did not explicitly write in Ref. 26 the generalized instability criterion [Eq. (7) of the present paper] but we have given the corresponding Feynman diagrams (Fig. 5) which are completely different from those of the standard model.

It should be stressed that we have obtained a generalized Stoner criterion without using a matrix representation as done in Refs. 32–34. To determine the correct instability criterion, the matrix representation *is not compulsory* contrary to what has been asserted in Refs. 33 and 34. Whatever the method used to derive it, the Stoner criterion should take into account the interplay between the two bands [χ_m' term in Eq. (9)]. Next, we show that the Stoner criterion given by Eq. (7) is exactly equivalent to that deduced from a model based on a matrix representation.

Let us write the Stoner criterion [Eq. (7)] for both the m and the $\bar{m}$ bands:

$$\frac{1}{g_0} = \frac{1}{2}\chi_m^0(\vec{Q}_m^0,T) + \frac{1}{2}\frac{g_b}{g_0}\chi_m'(2(k_F^{\bar{m}} - k_F^m),T),$$

$$\frac{1}{g_0} = \frac{1}{2}\chi_{\bar{m}}^0(\vec{Q}_{\bar{m}}^0,T) + \frac{1}{2}\frac{g_b}{g_0}\chi_{\bar{m}}'(2(k_F^m - k_F^{\bar{m}}),T).$$

Combining these two equations leads to

$$\left[1 - \frac{g_0}{2}\chi_m^0(q_0^m,T)\right]\left[1 - \frac{g_0}{2}\chi_{\bar{m}}^0(q_0^{\bar{m}},T)\right] - \frac{1}{4}g_b^2[\chi_m'(2(k_F^{\bar{m}} - k_F^m),T)]^2 = 0, \tag{10}$$

where we put $\chi_m' = \chi_{\bar{m}}'$ regarding the properties of the Ψ functions.[54]

In the zero field limit, the two bands are still separated by a gap depending on the V. In this case the Stoner criterion takes the same form as in the presence of a magnetic field and is also given by Eq. (10). It is worth noting that in Refs. 34 and 33, the Stoner criterion is also written in the same way either in the presence or in the absence of a magnetic field. We are then led to the instability criterion obtained by Sengupta and Dupuis in the absence of a magnetic field [Eq. (2.23) in Ref. 32] and which is calculated using a matrix representation for the spin susceptibilities. The χ_m^0 and the $\chi_{\bar{m}}^0$ terms in Eq. (10) correspond respectively to the diagonal terms $\chi^0(\vec{Q},\vec{Q})$ and $\chi^0(\vec{Q}+\vec{K},\vec{Q}+\vec{K})$ of Ref. 32, while the χ_m' is the off-diagonal component of the susceptibility $\chi^0(\vec{Q},\vec{Q}+\vec{K})$ reflecting the presence of the anion potential described by the wave vector $\vec{K}=(0,\pi/b)$. It is worth to note that the comparison of Eq. (2.23) of Ref. 32 and Eq. (10) of the present work with the Stoner criterion derived by Radić *et al.*[34] is not obvious since the definitions of the spin susceptibilities are not the same.

Let us now consider the case of a zero anion gap V. In this limit, the χ_m' term in Eq. (7) reduces to χ_m^0 while $g_0 = g_b$ and $q_0^m = 2k_F$. Equation (7) takes then the following from

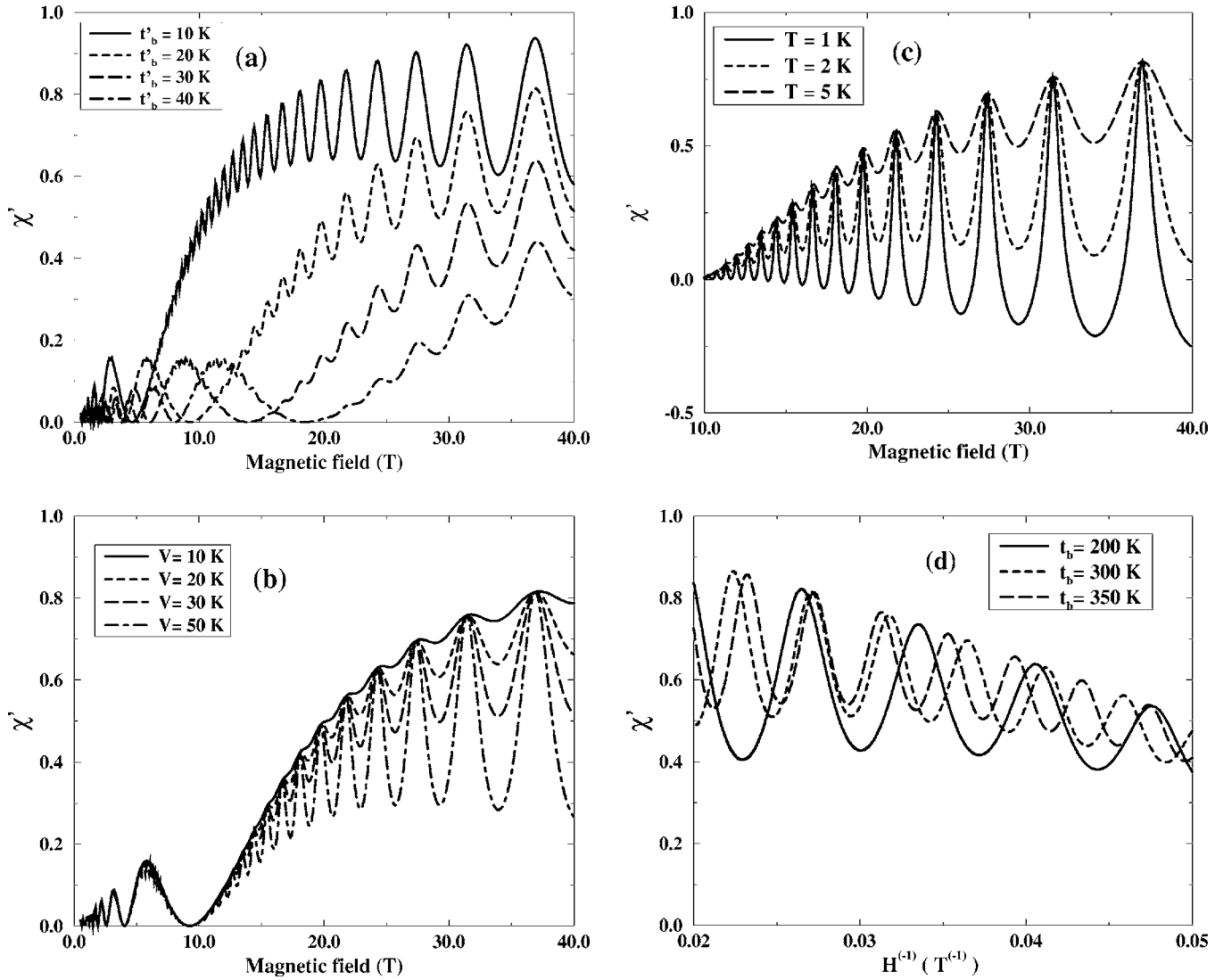

FIG. 6. Field dependence of the χ'_m [Eq. (9)] for different values of t'_b (a), V (b), temperature T (c), and t'_b. In the three cases t_b is fixed to 300 K. The calculations are done for $V=30$ K and $T=5$ K (a), $t'_b=20$ K and $T=5$ K (b), and $t'_b=20$ K and $V=30$ K (c). In (d), we have taken $t'_b=20$ K, $T=5$ K, and $V=30$ K.

$$1 - g_0 \chi^0_m(2k_F, T) = 0,$$

which is nothing but the Stoner criterion for a single band model as found within the QNM.[5]

In Fig. 6 we have represented the dependence of the χ'_m [Eq. (9)] on some key parameters. The figure shows that χ'_m oscillates as the magnetic field varies and the oscillations are more and more enhanced as the field increases. This reflects the dependence of χ'_m on the effective gap Δ [Eq. (3)] whose oscillation amplitude increases with increasing field.

Figure 6(a) shows that χ'_m is enhanced as t'_b increases. Moreover, the oscillation amplitude of χ'_m is also increased. To analyze this feature, one should keep in mind that χ'_m depends implicitly on t'_b through the I_n coefficients and in particular I_0 which is the dominant one for the $N=0$ phase. As I_0 increases with decreasing t'_b, the amplitude of χ'_m is found to be also increased. As a result the T_0 transition temperature, which is the solution of Eq. (7), is expected to increase as t'_b decreases. Indeed, an increase of the I_0 coefficient is equivalent to an enhancement of the coupling constants (g_0 and g_b) which leads to an increase of T_0.

Let us now turn to the oscillations of χ'_m. These oscillations originate from the dependence of the χ^{1D}_m factor on the effective anion gap Δ [Eq. (8)]. The amplitude of χ^{1D}_m is modulated essentially by the I_0 coefficient in the case of the $N=0$ phase. This coefficient, as we have said before, increases by decreasing t'_b, which induces an enhancement of the χ^{1D}_m amplitude and so an amplification of its oscillating behavior. This explains the pronounced oscillating character of χ'_m as t'_b decreases.

Figure 6(b) shows that the amplitude of the oscillations of χ'_m increases with V. This is once again related to the oscillating behavior of χ^{1D}_m. An increase of V induces an increase of the effective gap Δ [Eq. (3)] giving rise to larger oscillations of χ^{1D}_m according to Eq. (8).

In Fig. 6(c) we have depicted the behavior of χ'_m for different temperatures. As the temperature increases, the oscil-

lations are lowered since the thermal fluctuations are enhanced, which erase the effect of the gap Δ.

On the other hand, Fig. 6(d) shows the dependence of the χ'_m on the inverse of the magnetic field. The oscillation periodicity is reduced as t_b increases. For t_b=350 K, the periodicity is of the order of 250 T which is reminiscent of the experimental value 260 T. However, we cannot pretend, based on the behavior of χ'_m, to describe the exotic experimental feature of the rapid oscillations (RO) observed in $(TMTSF)_2ClO_4$.[20,18] The origin of the RO is actually subtle since such RO have been also reported in the case of $(TMTSF)_2PF_6$ which is, contrary to $(TMTSF)_2ClO_4$, characterized by a single band model. Therefore, one cannot ascribe the RO to the presence of a two band energy spectrum.

Let us now turn to the $N=1$ phase, which originates, as we have discussed above, from the interband scattering processes namely the g_f and the g_t terms in H_{int}^{MF} [Eq. (4)]. Since only one nesting vector is needed in this case to account for the SDW instability, then only one order parameter should be defined as

$$\Delta_1 = -g_f\langle\psi_{\bar{m}2\bar{\sigma}}(\vec{r})\psi^{\dagger}_{m1\sigma}(\vec{r})\rangle\exp^{i\vec{Q}_1\cdot\vec{r}},$$

where $\vec{Q}_1=(q_1,q_\perp^1)$. Here $q_1=2k_F+G$ denotes the longitudinal component of $\vec{Q}_1$ while $q_\perp^1$ is the transverse one which depends on the value of the magnetic field.

The interacting part of the mean field Hamiltonian in the $N=1$ phase reads then as

$$\begin{aligned}H_1^{MF} = &\sum_m\sum_\sigma\int d\vec{r}\{\Delta_1(\vec{r})\exp^{-i\vec{Q}_1\cdot\vec{r}}\psi_{\bar{m}1\sigma}(\vec{r})\psi^{\dagger}_{m2\bar{\sigma}}(\vec{r})\\ &+\Delta_1^*(\vec{r})\exp^{i\vec{Q}_1\cdot\vec{r}}\psi_{m2\bar{\sigma}}(\vec{r})\psi^{\dagger}_{\bar{m}1\sigma}(\vec{r})\}\\ &+\frac{g_t}{g_f}\sum_m\sum_\sigma\int d\vec{r}\{\Delta_1(\vec{r})\exp^{-i\vec{Q}_1\cdot\vec{r}}\psi_{m1\sigma}(\vec{r})\psi^{\dagger}_{\bar{m}2\bar{\sigma}}(\vec{r})\\ &+\Delta_1^*(\vec{r})\exp^{i\vec{Q}_1\cdot\vec{r}}\psi_{\bar{m}2\bar{\sigma}}(\vec{r})\psi^{\dagger}_{m1\sigma}(\vec{r})\},\end{aligned}$$

where

$$\Delta'_1 = -g_f\langle\psi_{\bar{m}2\uparrow}(\vec{r})\psi^{\dagger}_{m1\downarrow}(\vec{r})\rangle\exp^{i\vec{Q}_1\cdot\vec{r}}.$$

We define the following Green functions:

$$F_m^1(\bar{r},\bar{r}') = -\langle T_\tau[\psi_{m2\downarrow}(\bar{r})\psi^{\dagger}_{\bar{m}1\uparrow}(\bar{r}')]\rangle\exp^{i\vec{Q}_1\cdot\vec{r}},$$

$$G_m^1(\bar{r},\bar{r}') = -\langle T_\tau[\psi_{m1\downarrow}(\bar{r})\psi^{\dagger}_{\bar{m}1\uparrow}(\bar{r}')]\rangle.$$

Writing the motion equations of F_m^1 and G_m^1 we obtain the following Gor'kov's equations:

$$\begin{aligned}&\left[i\omega_n-\mu_BH+iv_F\frac{d}{dx}+v_Fk_F-\epsilon_\perp\left(p-\frac{x}{x_0}\right)\right]G_m^1\\ &\quad+\Delta_1^*\left[1+\frac{g_t}{g_f}\right]F_{\bar{m}}^1=\delta(x-x'),\end{aligned}$$

$$\begin{aligned}&\left[i\omega_n+\mu_BH-iv_F\frac{d}{dx}-\frac{v}{x_0}-v_Fk_F-\epsilon_\perp\left(p+q_\perp^1b-\frac{x}{x_0}\right)\right]\\ &\quad\times F_{\bar{m}}^1+\Delta_1\left[1+\frac{g_t}{g_f}\right]G_m^1=0.\end{aligned}$$

We introduce the following quantities:

$$\begin{aligned}f_m^1(x,x') = F_m^1(x,x')\exp\Bigg[&i\left(\frac{\mu_BH}{v_F}-k_F\right)(x-x'-\frac{i}{v_F}\int_0^x\epsilon_\perp\\ &\times\left(p-\frac{u}{x_0}-q_\perp^1b\right)du-\frac{i}{v_F}\int_0^{x'}\epsilon_\perp\left(p-\frac{u}{x_0}\right)du\Bigg],\end{aligned}$$

$$\begin{aligned}g_m^1(x,x') = G_m^1(x,x')\exp\Bigg[&-i\left(\frac{\mu_BH}{v_F}-k_F\right)(x-x')\\ &+\frac{i}{v_F}\int_{x'}^x\epsilon_\perp\left(p-\frac{u}{x_0}\right.\\ &\left.-q_\perp^1b\right)du-\frac{i}{v_F}\int_0^{x'}\epsilon_\perp\left(p-\frac{u}{x_0}\right)du\Bigg],\end{aligned}$$

$$\begin{aligned}\tilde{\Delta}_1(x,p) = \Delta_1^*(x)\exp\frac{i}{v_F}\Bigg[&\int_0^x\epsilon_\perp\left(p-\frac{u}{x_0}-q_\perp^1b\right)du\\ &+\int_0^x\epsilon_\perp\left(p-\frac{u}{x_0}\right)du\Bigg].\end{aligned}$$

The Gor'kov's equations read then as

$$\left(i\omega_n+iv_F\frac{d}{dx}\right)g_m^1+\tilde{\Delta}_1\left[1+\frac{g_t}{g_f}\right]f_{\bar{m}}^1=\delta(x-x'),$$

$$\left(i\omega_n-iv_F\frac{d}{dx}-\frac{v}{x_0}\right)f_{\bar{m}}^1+\tilde{\Delta}_1^*\left[1+\frac{g_t}{g_f}\right]f_m^1=0.$$

As in the case of the $N=0$ state, we consider the Fourier expansion of $f_m^1(x,x')$ and $g_m^1(x,x')$ for which the jth Fourier component, respectively denoted by $f_j^{m(1)}(k,\omega_n)$ and $g_j^{m(1)}\times(k,\omega_n)$, satisfy

$$(i\omega_n-v_Fk)g_1^{m(1)}(k,\omega_n)+\sum_j(\delta_j^1)^*\left[1+\frac{g_t}{g_f}\right]f_j^{\bar{m}(1)}(k,\omega_n)=1,$$

$$(i\omega_n+v_Fk)f_1^{\bar{m}(1)}(k,\omega_n)+\sum_j\delta_j^1\left[1+\frac{g_t}{g_f}\right]g_j^{m(1)}(k,\omega_n)=0,$$

with $\delta_n^1=I_n(q_\perp^1)\Delta_1$.

The self-consistency condition is given by

$$\Delta_1 = g_fT\sum_{\omega_n}\langle F_m^1(x,x',p,\omega_n)\rangle_p,$$

We, then, obtain the following Stoner criterion for the $N=1$ phase:

$$\frac{1}{g_f}=\frac{1}{2}\left[1+\frac{g_t}{g_f}\right]\chi_1(\vec{Q}_1,T), \tag{11}$$

where $\chi_1(\vec{Q}_1,T)$ is the susceptibility of the $N=1$ phase:

$$\chi_1(\vec{Q}_1,T)=\sum_n I_n^2(q_\perp^1)\chi^{1\mathrm{D}}(q_1-nG,T).$$

$\chi^{1\mathrm{D}}$ is the bare susceptibility of a one-dimensional system showing logarithmic divergences at $q_x=2k_F+nG$:

$$\chi^{1D}(q_x)=N(0)\left[\ln\left(\frac{2\gamma E_0}{\pi T}\right)+\Psi\left(\frac{1}{2}\right)-\mathrm{Re}\,\Psi\left(\frac{1}{2}+i\frac{v_F(q_x-2k_F)}{4\pi T}\right)\right].$$

This expression is the same as that obtained for a single band quasi-one-dimensional system since the $N=1$ phase originates from interband processes.

If $g_t=g_f$, we recover from Eq. (11) the Stoner criterion of quasi-one-dimensional system with only one band in its dispersion relation as in the $(TMTSF)_2PF_6$ salt. It is worth noting that, for the odd-N phases, one may obtain the following instability criterion:

$$\frac{1}{g_f}=\frac{1}{2}\left[1+\frac{g_t}{g_f}\right]\chi_N(\vec{Q}_N,T),$$

where $\chi_N(\vec{Q}_N,T)=\Sigma_n I_n^2(q_\perp^N)\chi^{1\mathrm{D}}(q_N-nG,T)$, q_N is the longitudinal component of the nesting vector of the N phase: $q_N=2k_F+NG$ and $q_\perp^N$ is the transverse one.

As shown by the Stoner criteria obtained in Eq. (7) and (11), the coupling constants g_μ, $(\mu=0,f,t,b)$ play a crucial role for the stability of the $N=0$ and the $N=1$ phases. In the random phase approximation (RPA), one may expect to have the same value $g_\mu=g$ for the different coupling processes. However, in the following, we will show, within a renormalization group approach, that depending on the value of the anion gap, the coupling constants may be differently renormalized.

IV. RENORMALIZATION OF THE COUPLING CONSTANTS

It has been shown that the perturbative renormalization group (PRG) method is well suited to explore quasi-one-dimensional systems with a two band dispersion relation as the two-coupled-chain model[52] or spin ladder systems.[55] The renormalization technique is used to take into account the influence of the high-energy states on the scattering processes at lower energy.[56]

At high temperature, the phase diagram of the quasi-one-dimensional organic conductors shows the presence of a one dimensional phase with a non-Fermi liquid character. By decreasing the temperature, the electron motion along the **b** direction is deconfined and the interchain hopping process t_b becomes coherent. At a critical temperature T_{cross}, the system undergoes a dimensional crossover from the 1D phase to a 2D (or 3D) Fermi liquid state. Due to its two-band Fermi surface, the relaxed ClO_4 salt may be regarded as a set of two coupled chains (ladder) interacting via one particle hopping processes t_b and t_b'.

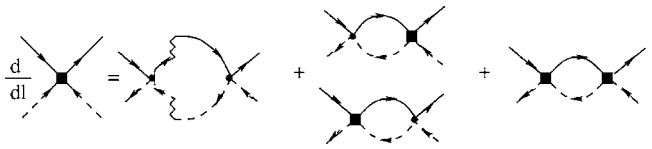

FIG. 7. First order diagrams for two particle hopping amplitudes in the SDW channel. The dots represent the coupling strengths $g_\mu^{(2)}$, the squares denote the V_μ processes, and the zigzag line corresponds to the one particle hopping process t_b, after Ref. 55.

Within a weak coupling RG approach, the coupled chains model has been discussed in Ref. 52 taking into account the g_b process. The effect of an interladder hopping parameter has been studied in Ref. 55. In this section, we shall determine the renormalization couplings based on the models of those references.

The g_μ $(\mu=0,f,t,b)$ coupling constants which appear in the Stoner criteria [Eqs. (7) and (11)] are the renormalized couplings G_μ^* deduced from the 1D renormalization procedure carried out down to T_{cross}:

$$g_\mu=G_\mu^*=G_\mu(T_{\mathrm{cross}}),$$

where G_μ is given by[58,57]

$$G_\mu(T_{\mathrm{cross}})=V_\mu(T_{\mathrm{cross}})-g_\mu^{(2)}(T_{\mathrm{cross}}).$$

$g_\mu^{(2)}$ are the 1D two particle scattering amplitude in the forward channel and V_μ denote pair tunneling amplitude between two couples of interacting chains within the SDW channel.[55]

A. Scaling equations

The method we have adopted to derive the perturbative renormalization group equations is that developed by Bourbonnais and Caron.[57,58] Within this method the temperature is parametrized as $T(l)=E_0e^{-l}$ where l is the scaling parameter and E_0 is the bandwidth cutoff, which is of the order of the Fermi energy.

To the one loop level, the scaling of the two particle processes $g_\mu^{(2)}$ $(\mu=0,f,t,b)$ and the hopping parameter t_b are given in the Appendix. During the RG procedure, t_b grows as l increases and becomes of the order of E_0 at a some critical value of the scaling parameter l_{cross} defined by $t_b(l_{\mathrm{cross}})=E_0$ which gives the crossover temperature $T_{\mathrm{cross}}=E_0e^{-l_{\mathrm{cross}}}$ as introduced by Bourbonnais and Caron.[57,58] Beyond l_{cross}, the perturbative RG treatment breaks down since t_b can no more be considered as a perturbation. The RG equations of the V_μ processes are represented in Fig. 7.

The scaling equations then read as

$$\frac{dV_0}{dl}=\frac{1}{4}[\tilde{t}_b(l)g_0^{(2)}(l)]^2\cos q_\perp+g_0^{(2)}(l)V_0(l)-\frac{1}{2}V_0(l)^2+\frac{1}{4}[\tilde{t}_b(l)g_b^{(2)}(l)]^2\cos q_\perp+g_b^{(2)}(l)V_b(l)-\frac{1}{2}V_b(l)^2,$$

$$\frac{dV_f}{dl} = -\frac{1}{4}\tilde{t}_b(l)^2[(g_t^{(2)}(l))^2 + (g_f^{(2)}(l))^2]\cos q_\perp + g_t^{(2)}(l)V_t(l) + g_f^{(2)}(l)V_f(l) - \frac{1}{2}[V_t(l)^2 + V_f(l)^2],$$

$$\frac{dV_t}{dl} = -\frac{1}{2}\tilde{t}_b(l)^2 g_t^{(2)}(l) g_f^{(2)}(l)\cos q_\perp + g_t^{(2)}(l)V_f(l) + g_f^{(2)}(l)V_t(l) - V_t(l)V_f(l),$$

$$\frac{dV_b}{dl} = \frac{1}{2}\tilde{t}_b(l)^2 g_b^{(2)}(l) g_0^{(2)}(l)\cos q_\perp + g_b^{(2)}(l)V_0(l) + g_0^{(2)}(l)V_b(l) - V_0(l)V_b(l). \quad (12)$$

Here, $q_\perp = \pi$ since V_μ correspond to the SDW channel.

It should be noted that we did not take into account the magnetic field when deriving the scaling equations since, at high temperature, thermal fluctuations are much greater than the magnetic energy.[59] A more detailed RG analysis including both the effect of temperature and the magnetic field will be discussed in a forthcoming paper.

The scaling equations of the $g_\mu^{(2)}$ are given in the Appendix. It should be noted that the RG equations in Ref. 55 do not include the g_b and the V_b terms.

We solved the scaling equations (A1) and Eqs. (12) with the initial condition:

$$g_\mu^{(1)}(0) = g^{(1)}(0), \quad g_\mu^{(2)}(0) = g^{(2)}(0) \text{ and } V_\mu = 0,$$

where $g_\mu^{(1)}$ are the scattering amplitudes in the backward channel. The renormalization is carried out from E_0 to T_{cross}. We have to note that in the mean field approach of FISDW phases, the $g_\mu^{(1)}$ processes may be neglected. However, in the RG procedure, the renormalization of the $g_\mu^{(2)}$ depends on the $g_\mu^{(1)}$ couplings.

The numerical results show that, the difference between the intraband renormalized couplings (G_0^*, G_b^*) and the interband ones (G_f^*, G_t^*) increases with increasing anion gap V. In Fig. 8, we have represented the dependence of the ratio $\langle G_{\text{inter}}\rangle/\langle G_{\text{intra}}\rangle$ on the anion gap V, where $\langle G_{\text{inter}}\rangle$ ($\langle G_{\text{intra}}\rangle$) is the mean value of the interband (intraband) renormalized coupling constants. We have considered the case where the bare couplings $g^{(1)}(0)$ and $g^{(2)}(0)$ are equal and that for different couplings, which amounts to take into account the Coulomb interaction to the second-nearest neighbors.[58,60]

Figure 8 shows that interband couplings are substantially greater than the intraband ones. It is worth stressing that, contrary to what Radić *et al.* have claimed in Ref. 34, we have taken in Ref. 26 a larger interband coupling constant than the intraband one.

As shown in Fig. 8, the larger the anion gap, the greater the difference between the two types of the scattering strengths. This difference depends on the bare coupling $g^{(1)}\times(0)$ and $g^{(2)}(0)$. It is found to be enhanced as the ratio $g^{(2)}(0)/g^{(1)}(0)$ increases.

For $V \sim 50$ K, the interband coupling is 30% larger than the interband one for $g^{(2)}(0) = g^{(1)}(0) = 0.6$ while it is 50% greater for $g^{(2)}(0)/g^{(1)}(0) = 1.2$. Such value is somewhat overestimated since we have considered one-loop scaling equations. However, it remains important even if we include second order RG corrections since the leading behavior is due to the one-loop terms.[58,59,61]

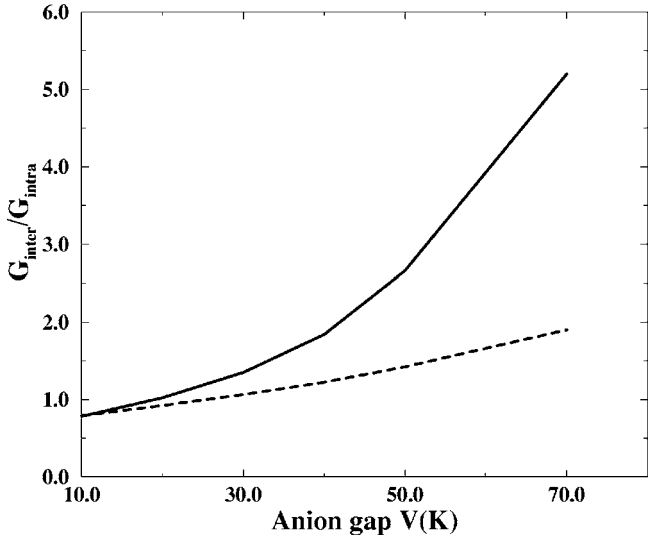

FIG. 8. The dependence of the ratio $\langle G_{\text{inter}}\rangle/\langle G_{\text{intra}}\rangle$ of the interband coupling and the intraband one on the anion gap V. The dashed line corresponds to equal bare couplings $[g^{(1)}(0) = g^{(2)}(0) = 0.6]$ while the solid one is obtained for different couplings $[g^{(1)}\times(0) = 0.45$ and $g^{(2)}(0) = 0.6]$. The calculations are done for $E_F = 3600$ K, $t_b = 200$ K, and $T_{\text{cross}} = 170$ K.

Our results are confirmed by the calculations of Abramovici *et al.*[62,63] who studied a ladder system within the one particle irreducible formalism of the RG method. The authors have reported that the renormalized interband couplings ($g_f^{(2)}$ and $g_t^{(2)}$) are greater than the intraband ones ($g_0^{(2)}$ and $g_b^{(2)}$) even if the gap separating the two bands is small. Moreover, they have found that the difference is enhanced if they take into account the dependence of the coupling constants $g_\mu^{(i)}$ $(i = 1,2; \mu = 0, f, t, b)$ on the longitudinal momentum k of the scattered particles. Such dependence is not included in the present work and is beyond the scope of this paper.

It comes down that, at the 1D-2D crossover temperature T_{cross}, the renormalized interband and intraband coupling strengths are different either for small or large anion gap V. The difference increases with increasing V. This effect has been neglected in Ref. 34 although the authors argued that V is as large as t_b. In this reference, the authors asserted that taking different couplings, as we have done in Ref. 26, is not justified for small V and was just put by hand to construct the phase diagram (Fig. 4 of Ref. 26). The numerical results obtained from the present RG study and those of Refs. 62 and 63 indicate clearly that the renormalization effect does exist even for small V and is enhanced as the bare couplings $g^{(1)}(0)$ and $g^{(2)}(0)$ increase.

In the following, we will show that, to obtain the temperature-field phase diagram, taking different couplings is not compulsory in our model. This contradicts the comment of Radic *et al.*[34] on our calculations of Ref. 26. Indeed, we will see that the qualitative features of the phase diagram

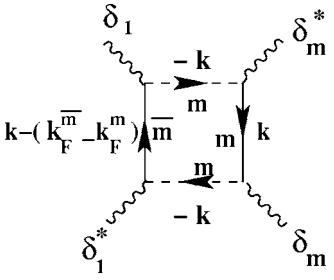

FIG. 9. Diagrammatic representation of the coexisting term of the total free energy [Eq. (13)]. $\delta_1=I_1\Delta_1$ and $\delta_m=I_0\Delta_0^m$. $(m=A,B)$.

are kept even for equal couplings (i.e., unrenormalized scattering strengths). To study the relative stability of the $N=0$ and the $N=1$ phases, we derive in the next section the Ginzburg-Landau expansion of the free energy.

V. THERMODYNAMICS

We have shown that the $N=0$ phase originates from intraband nesting processes while the $N=1$ phase is due to interband ones. The former induces two nesting vectors q_A^0 and q_B^0 whereas the latter depends on a single nesting vector q_1.

Within the Ginzgurg-Landau treatment, one should define, for the $N=0$ phase, *two* order parameters Δ_0^A and Δ_0^A respectively for the A band and the B band, which are given by

$$\Delta_0^A = -\langle \Psi_{A2\uparrow}^+ \Psi_{A1\downarrow}\rangle \exp^{iq_A^0 x},$$

$$\Delta_0^B = -\langle \Psi_{B2\uparrow}^+ \Psi_{B1\downarrow}\rangle \exp^{iq_B^0 x}.$$

However, only one order parameter is necessary for the $N=1$ phase, which is given by

$$\Delta_1 = -\langle \Psi_{A2\uparrow}^\dagger \Psi_{B1\downarrow}\rangle \exp^{iq_1 x}.$$

It should be stressed that both gaps Δ_0^A and Δ_0^B open *simultaneously* on the A band and the B band, respectively.

The total free energy F_T of the system compared to that of the normal state F_{norm} is given, up to the quartic order, by

$$F_T - F_{norm} = \frac{a_0}{2}(\Delta_0^A)^2 + \frac{a_0}{2}(\Delta_0^B)^2 + \frac{b_0}{2}(\Delta_0^A)^4 + \frac{b_0}{2}(\Delta_0^B)^4 + c_0(\Delta_0^A)^2(\Delta_0^B)^2 + a_1(\Delta_1)^2 + b_1(\Delta_1)^4 + \frac{d_{01}}{2}(\Delta_1)^2[(\Delta_0^A)^2 + (\Delta_0^B)^2]. \quad (13)$$

The last term in Eq. (13), which expresses the coexistence of the $N=0$ and the $N=1$ phases, corresponds to the fourth order diagram given by Fig. 9.

The d_{01} coefficient is given by

$$d_{01} = \frac{I_0^2 I_1^2}{4\pi\Delta T} M'\left(\frac{\Delta}{2\pi T}\right),$$

where $M'(x)$ is defined as[53]

$$M(x) = \frac{1}{2}\left[\Psi\left(\frac{1}{2}+ix\right) + \Psi\left(\frac{1}{2}-ix\right)\right],$$

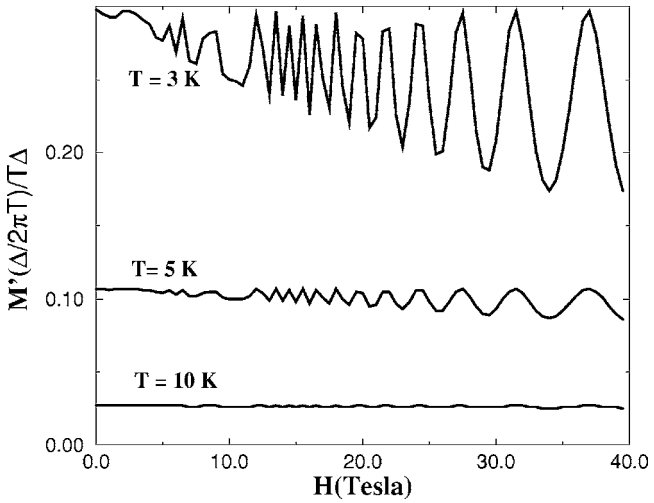

FIG. 10. The magnetic field dependence of the factor $[M'(\Delta/2\pi T)]/\Delta T$, which determines the sign of the coupling term d_{01}. The calculations are done for different temperatures.

$$M' = \frac{dM(x)}{dx}.$$

The dependence of d_{01} on the magnetic field for different temperatures is depicted in Fig. 10, which shows that d_{01} is positive for any value of the magnetic field.

Hence, the coupling term d_{01} will lead to an increase of the total free energy. This means that the minimized free energy will correspond to either the $N=0$ phase $(\Delta_1=0)$ or to the $N=1$ phase $(\Delta_0^A=\Delta_0^B=0)$ but not to the case where both of them coexist. Therefore, to study the competition between the $N=0$ phase and the $N=1$ phase, one should compare their corresponding free energies F_0 and F_1 given by

$$F_0 - F_{norm} = \frac{a_0}{2}(\Delta_0^A)^2 + \frac{a_0}{2}(\Delta_0^B)^2 + \frac{b_0}{2}(\Delta_0^A)^4 + \frac{b_0}{2}(\Delta_0^B)^4 + c_0(\Delta_0^A)^2(\Delta_0^B)^2, \quad (14)$$

$$F_1 - F_{norm} = a_1(\Delta_1)^2 + b_1(\Delta_1)^4. \quad (15)$$

The a_0 coefficient is given by the diagrams of Fig. 5 which give rise to the instability criterion of the $N=0$ phase [Eq. (7)]. The coefficients b_0 and c_0 of the fourth order terms in Eq. (14) are deduced from the diagrams of Fig. 11 and are written as

$$b_0 = \frac{I_0^4}{16\pi^2 T^2}\left[14\zeta(3) + M''\left(\frac{a}{\pi T}\right)\right],$$

$$c_0 = \frac{I_0^4}{4\pi T\Delta} M'\left(\frac{\Delta}{\pi T}\right), \quad (16)$$

where $M''(x)=d^2M(x)/dx^2$ and ζ is the zeta function.

Figure 12 shows the dependence of c_0 on the magnetic field. The main features deduced from this figure is that c_0 is positive and oscillates as the field is varied. This behavior is a key issue for the formation of the $N=0$ phase. The positive

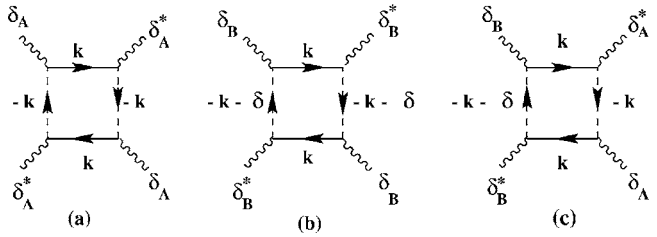

FIG. 11. Diagrammatic representation of the fourth order terms of the free energy in the $N=0$ state [Eq. (14)]. $\delta=4\Delta/v_F$ where Δ is the effective anion gap $\Delta=VJ_0(4t_b/v_FG)$ and $\delta_m=I_0\Delta_0^m$ $(m=A,B)$. The b_0 term is given by the (a) and (b) diagrams while the c_0 term corresponds to the (c) diagram.

sign of c_0 means that the coupling term in Eq. (14) will enhance the free energy.

From Fig. 12(a), we can conclude that by decreasing temperature, the coupling term is enhanced and, then, the destabilization of the $N=0$ phase is made more and more possible.

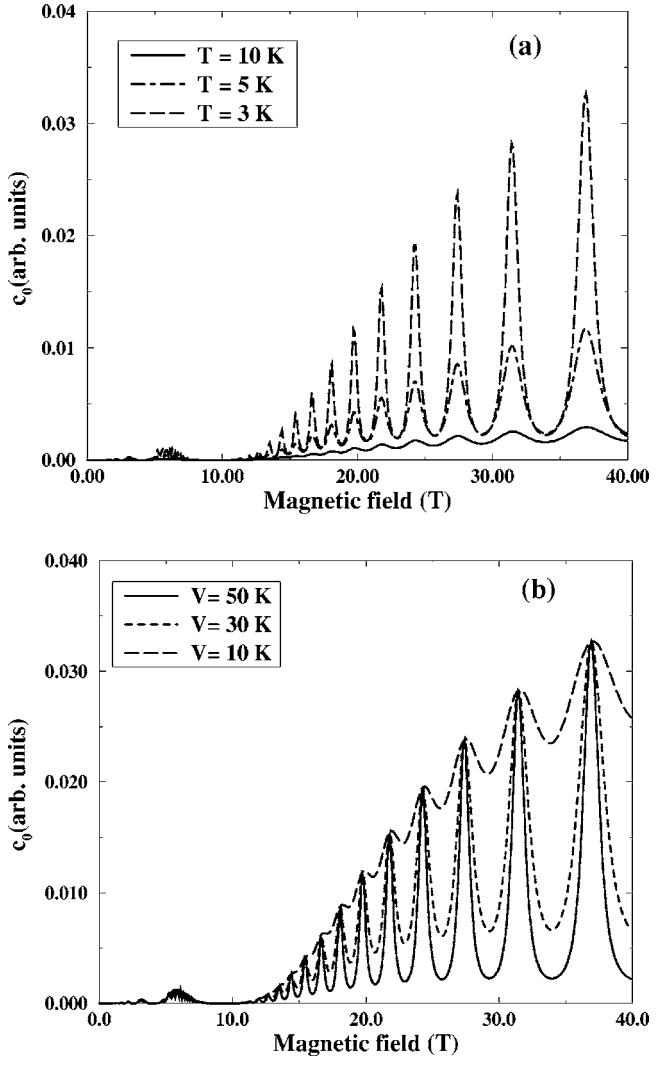

FIG. 12. The magnetic field dependence of the coupling term c_0 [Eq. (16)] in arbitrary units. In (a) the calculations are done for different temperatures and for $V=50$ K while in (b), the temperature is fixed at $T=3$ K and V is varied.

On the other hand, the increase of the anion gap V yields to a decrease of the minima of the c_0 term, for which the $N=0$ phase is furthered [Fig. 12(b)]. Hence, increasing the anion gap will give rise to a reentrance of the $N=0$ phase as we will discuss in Sec. VI.

It comes out that, for the $N=0$ phase, the presence of two order parameters Δ_0^A and Δ_0^B, which cooperate to stabilize this phase, turns out to be critical due to their coupling term. The latter originates from the overlap of two SDW components in the same band m: one majority component which forms at the Fermi level k_F^m and a second minority component which is induced by the SDW instability taking place on the other band $\bar{m}$. Therefore, as the temperature decreases, the coexistence of two order parameters in the $N=0$ phase will destabilize this phase, which may eventually vanish.

Concerning the $N=1$ phase, the corresponding free energy does not depend on the effective gap Δ and the a_1 and b_1 coefficients are, as expected, the same as those of a single band system.[8] This phase may appear below the second order transition temperature T_1 from the metallic state to the $N=1$ phase. T_1 satisfies the Stoner criterion given by Eq. (11). However, as far as T_1 is lower than T_0, the $N=0$ phase is stable below T_0. By decreasing the temperature, the magnitudes of the order parameters Δ_0^A and Δ_0^B increase in the $N=0$ phase.[64] The coupling term in the F_0 expression is therefore enhanced, which puts at a disadvantage the $N=0$ phase. This phase persists at least for $T>T_1$ since $\Delta_1=0$. Below T_1, a competition takes place between the original $N=0$ phase and the $N=1$ phase. The latter, which has no chance to appear inside the $N=0$ phase in the case of $(TMTSF)_2PF_6$, may be stabilized in the $(TMTSF)_2ClO_4$ salt, at the expense of the $N=0$ phase due to the increase of the coupling term by decreasing temperature.

To check up the possibility that the $N=1$ phase may appear *inside* the $N=0$ phase, one should compare their minimized free energies. We set $\Delta_0^A=\Delta_0^B=\Delta_0$, since both gaps open simultaneously on the corresponding band and there is no particular scenario which favors one band or the other. We denote by $[F_0]_{\min}$ and $[F_1]_{\min}$ the minimized free energies with respect to Δ_0 and Δ_1, given by

$$[F_0]_{\min}=-\frac{1}{4}\frac{a_0^2}{b_0+c_0},$$

$$[F_1]_{\min}=-\frac{1}{4}\frac{a_1^2}{b_1}.$$

The $N=1$ phase will form if there exists a critical temperature T_1^* which realizes the following conditions (Fig. 13):

$$\text{at } T_1^*, \quad [F_0]_{\min}=[F_1]_{\min},$$

$$\text{at } T<T_1^*, \quad [F_1]_{\min}<[F_0]_{\min}. \tag{17}$$

We have solved numerically Eq. (17) and we found, as we will discuss in the next section, that it is possible to find a solution T_1^* at which the system undergoes a phase transition from the $N=0$ phase to the $N=1$ phase. During this transition, which is of a first order, the order parameter changes from Δ_0 to Δ_1, given by

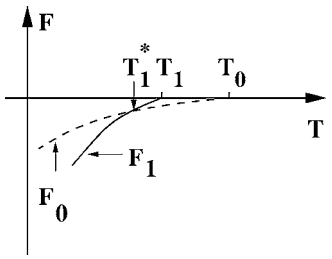

FIG. 13. Temperature dependence of the minimized free energies in the $N=0$ state ($[F_0]_{min}$) and the $N=1$ one ($[F_1]_{min}$). T_0 and T_1 are the solutions of Stoner criteria whereas T_1^* is deduced from Landau expansion of the free energies.

$$\Delta_0^2 = -\frac{a_0}{2(b_0+c_0)},$$

$$\Delta_1^2 = -\frac{a_1}{2b_1}.$$

Our calculations show that Δ_0 is smaller than Δ_1 for $T<T_1^*$. Therefore, in the coexisting regime ($T<T_1$), where both gaps coexist, the phase which forms is that corresponding to the largest gap. As argued by Yakovenko,[49] the Hall conductivity of a phase, where several order parameters coexist, is determined by the largest one. Hence, if the $N=1$ phase appears at T_1^* inside the $N=0$ phase, the Hall conductivity of this inner phase will be marked by a $N=1$ plateau, which is consistent with the experimental results.

Let us summarize the key issues of our proposed scenario. At T_0, a second order transition takes place from the metallic state to the $N=0$ phase. Simultaneously, two gaps Δ_0^A and Δ_0^B open on respectively the A band and the B band. Consequently, the whole Fermi surface becomes gapped. These two order parameters are coupled through the overlap of their corresponding SDW components. This coupling tends to destabilize the $N=0$ phase since it induces a positive term in the free energy which is found to be enhanced as the magnitudes of the order parameters increase with decreasing temperature. Eventually, a first order transition occurs at a critical temperature T_1^* from the original $N=0$ phase to the $N=1$ phase, which is characterized by a single order parameter Δ_1. This phase appears *inside* the $N=0$ phase and all the Fermi surface remains gapped. In the following, we discuss our numerical results and derive the high field phase diagram of the $(TMTSF)_2ClO_4$.

VI. RESULTS AND DISCUSSION

We have carried out the RPA calculations of Sec. III in the 2D regime ($T<T_{cross}$). We have solved numerically the Stoner criteria [Eqs. (7) and (11)] to determine the second order transition temperatures T_0 and T_1 from the metallic state to respectively the $N=0$ phase and the $N=1$ phase.

The key parameters on which depends the structure of the phase diagram are the hopping integrals t_b and t_b', the anion gap V and the coupling constants g_μ ($\mu=0,f,t,b$). In a first step, we disregard the renormalization effects and we assume that all the g_μ constants are equal.

A. Phase diagram with unrenormalized couplings

To derive the field-temperature phase diagram, we calculate the transition temperatures T_0 and T_1 from the Stoner criteria [Eqs. (7) and (11)] and the critical temperature T_1^* from Eq. (17). It should be kept in mind that T_{cross} is the characteristic energy of the 2D regime where the SDW instabilities take place. The bandwidth energy E_0 in the RPA is then replaced by T_{cross} and the coupling constants are those deduced from the renormalization procedure carried out in the 1D regime down to T_{cross}.[58] Taking $T_{cross}=150$ K, $t_b=300$ K, $t_b'=20$ K, and the dimensionless constants $g_\mu=g=0.47$, we have obtained the phase diagram of Figs. 14.

Figure 14(a) shows that the T_0 temperature increases with increasing field and tends to saturate at $T_0^{max}\sim 15$ K in the high field regime. Furthermore, the T_0 line exhibits an oscillating behavior as the magnetic field varies. The oscillations are less than 0.3 K which is consistent with experiments suggesting that any phase boundary oscillations are certainly less than 0.3 K. One should note that in Ref. 34, the transition line from the metallic state to the intraband phase shows in the high field regime deep oscillations which are of the order of the transition temperature. Such oscillations disagree with the experimental results.

In Fig. 14(b), we give the phase diagram for $V=30$ K. Here the oscillations of the T_0 line are enhanced but they do not exceed 0.7 K which is still in agreement with experiments.

In Fig. 14(c) we have represented the dependence of T_0 on the inverse of the magnetic field for different values of V. The figure shows that the greater the anion gap V, the larger the oscillations. Since no phase boundary oscillations have been reported experimentally, we can deduce from Fig. 14(c) that actually the anion gap should be small. In Sec. VI E we shall discuss in more details the dependence of these oscillations on the magnitude of V.

In Fig. 14(d) we checked the dependence of the oscillations on t_b. As we can note, the periodicity is affected by t_b but not by V [Fig. 14(c)]. This feature is due to the dependence of Δ on t_b [Eq. (3)] which governs its magnetic modulation. For $t_b=350$ K, $t_b'=20$ K, the periodicity deduced from the oscillations of the T_0 line is 250 T which fits the experimental value of 260 T reported from the RO. However, we cannot claim, within the present work, the existence of a clear relationship between the oscillation periodicity of T_0 and that of RO observed in magnetoresistance measurements. By the way, Radic *et al.*[34] have argued that the oscillations of their effective gap fit the experimental ones if V is of the order of t_b. This was the key argument used to justify the fact that V is large. Nevertheless, the periodicity of the effective gap is not necessary the same as that of the magnetoresistance. Indeed, Fig. 14(e) shows that the periodicity of T_0 and χ' [Eq. (9)] is different from that of the effective gap Δ.

It is worth to note that a recent experimental study has revealed a striking feature of the Hall resistance which shows large oscillations with sign reversal beyond 26 T an up to 45 T.[65] This behavior is reminiscent of Lebed's model concerning the ground state of $(TMTSF)_2ClO_4$ at very high magnetic field.[25] Lebed has shown that the energy gaps of

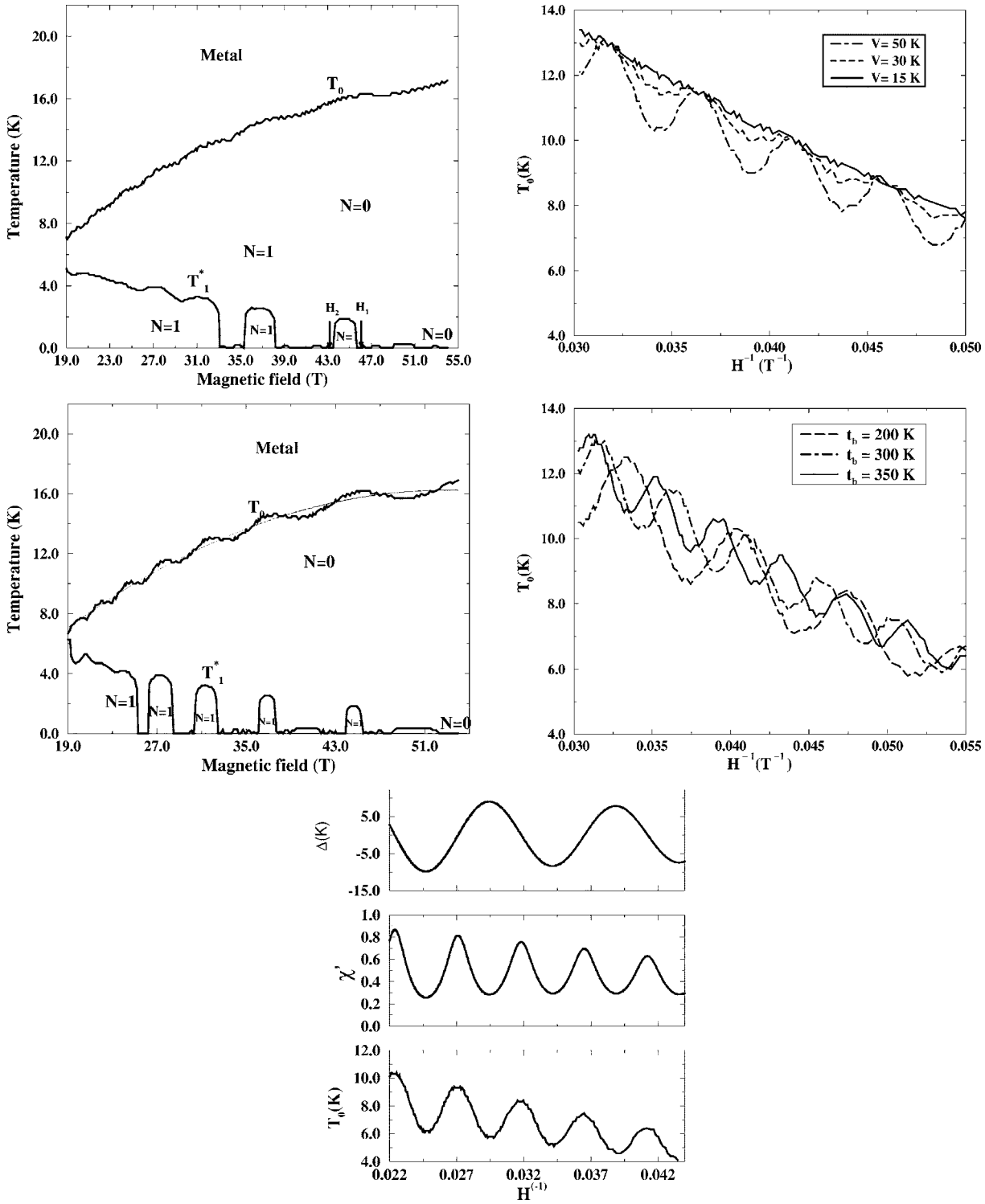

FIG. 14. (a) Temperature-field phase diagram of $(TMTSF)_2ClO_4$. The calculations are done for t_b=300 K, t_b'=20 K, V=19 K and for equal coupling constants g_μ=0.47. The oscillations of the T_0 line are less than 0.3 K. (b) Temperature-field phase diagram of $(TMTSF)_2ClO_4$. The calculations are done for t_b=300 K, t_b'=20 K, V=30 K and for equal coupling constants g_μ=0.47. The solid line T_0 is the fitted curve of the numerical data represented by the dashed line. The latter shows oscillations which do not exceed 0.7 K. (c) T_0 as a function of the inverse of the magnetic field for different V values. The calculations are done for t_b=300 K, t_b'=20 K and for equal coupling constants g_μ=0.47. (d) T_0 as a function of the inverse of the magnetic field for different t_b values. The calculations are done for t_b'=20 K, V=50 K and for equal coupling constants g_μ=0.47. (e) Δ(a), χ' and T_0 as a function of the inverse of the magnetic field. The calculations are done for t_b=300 K, t_b'=20 K, V=50 K and with g_0=0.39 for the intraband coupling constant.

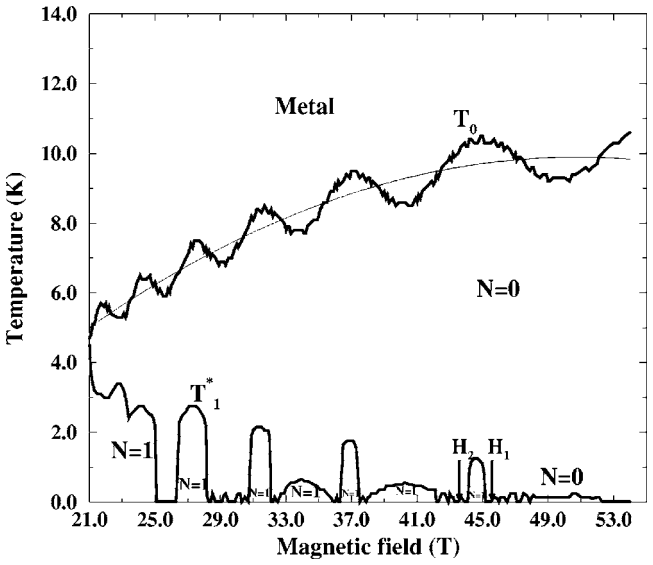

FIG. 15. Temperature-field phase diagram of $(TMTSF)_2ClO_4$. The calculations are done for $t_b=300$ K, $t'_b=20$ K, $V=30$ K, $g_1=0.43$ and $g_0=0.39$. The dashed line is a fit of the T_0 line. The oscillations of the latter are of the order of 0.8 K.

the FISDW phases are periodic on the inverse of the magnetic field. However, this model cannot explain the formation of the FISDW states appearing at moderate magnetic field (SDWI, SDWII, SDWIII, SDWIV in Fig. 1). Further theoretical investigations are needed to interpret the RO phenomenon in particular at high magnetic field.

Let us turn to Fig. 14(a) which shows that, by decreasing the temperature, a first order transition takes place at $T^*_1 \sim 3$ K from the $N=0$ phase to the $N=1$ phase. The T^*_1 transition line collapses at a critical field $H_1 \sim 45$ T. Experimentally, this field value is about 27 T at which the inner boundary line, found by McKernan *et al.* ends.

Comparing quantitatively our proposed phase diagram with the experimental ones, it seems that only T_0, which is of the order of 15 K, is somewhat in discrepancy with the 5.5 K phase boundary. However, it should be kept in mind that T_0 is derived from RPA calculations and so the real transition temperature is much smaller. This discrepancy is quite reduced if we take into account the renormalization effects on the coupling strengths as discussed in Sec. IV.

In the following we derive the phase diagram corresponding to different coupling constants.

B. Phase diagram with renormalized couplings

We have carried out the calculations considering different coupling constants for the interband and the intraband scatterings. The phase diagram of Fig. 15 is obtained with the same data as in Fig. 14 except that we have taken $g_0=0.39$ and $g_1=0.43$ for respectively the intraband couplings and the interband ones. This gives rise to difference of the order of 10 % in the coupling magnitude which is consistent with the RG results of Sec. IV.

Figure 15 shows that the quantitative agreement between the calculated phase diagram and experiments is improved if we take different coupling constants. Indeed, the T_0 boundary line saturates, in this case, at 9 K which is consistent with the 5.5 K transition line.

It should be noted that, in this case T_0 is lower than that obtained in the case of equal coupling constant [Fig. 14(a)] but the corresponding oscillations, which are of the order of 0.9 K, are greater. This can be understood from the behavior of the χ'_m term [Eq. (9)]. As shown in Fig. 12(b), by decreasing the temperature the oscillation amplitude of χ'_m increases, which enhances the T_0 oscillating behavior. In the following we discuss in details the different features of the obtained phase diagrams.

C. Discussion

Figures 14 and 15 show that the second order transition temperature T_0 increases with the magnetic field and saturates in the high field regime. This behavior is reminiscent of the 5.5 K boundary line obtained experimentally.[16,19,20] The saturation behavior of the T_0 line depends on both the anion gap V and the ratio t'_b/t_b. The T_0 line may show, as we will see later, phase boundary oscillations which are enhanced with increasing V and may become important for V larger than 60 K. In Ref. 34, the obtained critical temperature starts to oscillates as the magnetic field increases. Such oscillations have not been observed experimentally down to 0.3 K, which supports the assumption of a small anion gap.

As shown in Figs. 14 and 15, below the first order transition line T^*_1, the $N=1$ phase forms *inside* the original $N=0$ SDW phase. In this inner phase, both order parameters Δ_0 and Δ_1 coexist but Δ_1 is the largest. One should, then, expect a $N=1$ plateau in the Hall conductivity of the inner phase as discussed above.

At H_1, a first order transition takes place from the $N=1$ phase (SDW III in Fig. 1) to the high field $N=0$ insulating state (SDW II in Fig. 1) as found experimentally.[16,20] Above H_1, the T^*_1 line vanishes whereas the T_0 one persists and tends to become field independent.

The presence of a second critical field H_2 at which the T^*_1 line vanishes, is consistent with the experimental results of Moser *et al.*[19] and Chung *et al.*[20] showing that T^*_1 line goes to zero at 17 T. The collapse of the T^*_1 boundary at H_2 and the reentrance of the $N=0$ phase is due to the dependence of the coupling coefficient c_0 [Eq. (16)] on the magnetic field. As shown in Fig. 12, the c_0 has minima at given field values for which the coupling term in the expression of the $N=0$ free energy F_0 is reduced. The competition between the $N=0$ phase and the $N=1$ one may turn in favor of the $N=0$ phase at these minima. This will depend on the magnitude of the order parameters. As we will see in the next sections, the number of the critical field values at which one may have a reentrant $N=0$ phase depends on several parameters such as the imperfect nesting parameter t'_b and the anion gap V.

According to Figs. 14 and 15 the $N=1$ phase is still present in the low field regime. Therefore, the SDW IV phase in Fig. 1 corresponds the $N=1$ phase. This is consistent with the experimental phase diagram of Chung *et al.*[20]

It turns out that, within the present treatment, we are able to label the different subphases of the $(TMTSF)_2ClO_4$ in the

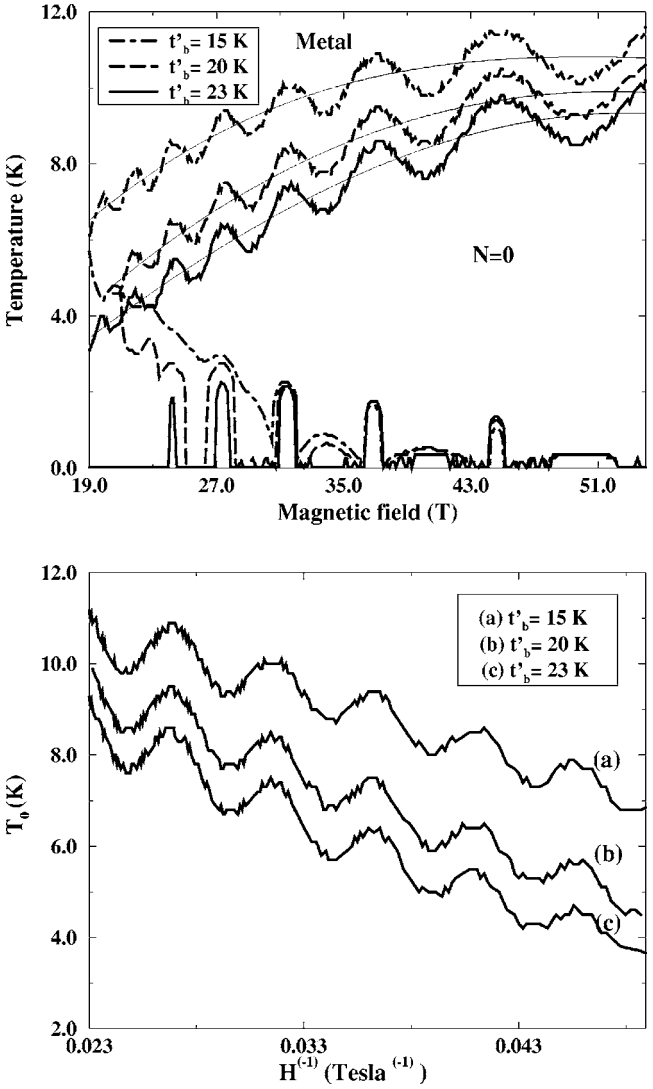

FIG. 16. (a) Temperature-field phase diagram of $(TMTSF)_2ClO_4$ for different values of the unnesting parameter t_b'. The calculations are done for $t_b=300$ K, $V=30$ K, $g_1=0.43$ for the interband coupling and $g_0=0.39$ for the intraband ones. The lines of the same type correspond to a given t_b'. The set of the upper lines are ascribed to the T_0 lines while the bottom ones are associated to the T_1^* phase boundaries. The thin solid lines are the fitted curves of T_0 lines. (b) T_0 transition temperature as a function of the inverse of the magnetic field for different values of the imperfect nesting parameter t_b'. The data are the same as in (a).

high field regime. We can then conclude that the inner phases SDWIII and SDWIV in Fig. 1 correspond to the same semimetallic $N=1$ FISDW phase but they are completely different from the high field insulating state (SDWII) which is associated to the $N=0$ FISDW phase.

In the next section we will focus on the dependence of the phase diagram on some key parameters in particular the unnesting parameter t_b' and the anion gap V.

D. High field phases and the imperfect nesting parameter t_b'

In Fig. 16(a) we show the phase diagram of the $(TMTSF)_2ClO_4$ for different values of the unnesting parameter t_b'. By decreasing t_b', the T_0 transition temperature increases. This behavior is similar to that obtained within the QNM for a single band model as in $(TMTSF)_2Pf_6$. T_0 depends substantially on the I_0 factor [Eq. (7)]. The latter increases as the t_b/t_b' ratio increases leading to an enhancement of T_0.[5]

One should note that the tendency to saturation of the T_0 boundary line at high field depends on the value of t_b'. With increasing t_b', the saturation of T_0 is more and more difficult to reach. This behavior is reminiscent of the experimental results of Matsunaga *et al.* in the case of deuterated[66] $(TMTSF)_2ClO_4$.[50]

The oscillating behavior of the T_0 phase boundary is expected to be more and more pronounced as t_b' decreases. This originates from the dependence of the χ_m' term on t_b' [Fig. 6(a)]. On the other hand, T_0 is pushed to higher temperature as t_b' decreases. However, as the temperature increases, the oscillation amplitude of χ_m' decreases [Fig. 6(c)]. Therefore, the oscillations of the T_0 line will depend of the competition between the unnesting parameter t_b' and the thermal fluctuations. It is worth noting that the oscillation periodicity of T_0 is unchanged as t_b' varies since the effective gap Δ is independent of t_b' [Fig. 16(b)].

Concerning the inner phase, it seems that as t_b' increases, the reentrance of the $N=0$ phase is furthered and the $N=1$ phase is found to be shifted to lower field. This can be understood from Eq. (16) according to which the coupling term c_0 decreases with decreasing I_0. As we have discussed in Sec. V, a decrease of c_0 stabilizes the $N=0$ phase. Therefore, as t_b' increases, the c_0 factor is lowered and the reentrance of the $N=0$ phase is furthered at the expense of the $N=1$ phase. For the chosen data of Fig. 16, we found that the $N=1$ phase disappears for t_b' larger than 25 K and only the original $N=0$ phase persists in the high field regime.

E. High field phases and the anion gap

Figure 17 shows the dependence of the high FISDW phases on the magnitude of the anion gap V. The metal-$N=0$ boundary line T_0 is found to be lowered as V increases. This is due to the dependence on V of the generalized Stoner criterion [Eq. (7)] through the χ_m' term. From Eq. (9) we deduce that, the larger the anion gap V, the larger the deviation from perfect nesting, the lower the transition temperature T_0.

Furthermore, the oscillations of the T_0 phase boundary are enhanced as V increases. This is due to the presence of the χ_m' term in the Stoner criterion [Eq. (7)]. Increasing V yields to an increase of the oscillation amplitude of χ_m' [Fig. 6(b)].

From Fig. 17 we note that, as V increases, the inner phase spreads out on a larger range and its boundary line T_1^* is shifted to higher temperature. It should be stressed that, the metal-$N=1$ transition line T_1 [Eq. (11)] is V independent. However, as V increases the T_0 temperature decreases which puts at disadvantage the $N=0$ phase and enhances the T_1^* critical temperature given by Eq. (17).

As shown in Fig. 17, increasing V furthers the reentrance of the $N=0$ phase. This is due to the fact that the minima of the coupling term c_0 [Eq. (16)] decreases as V increases [Fig.

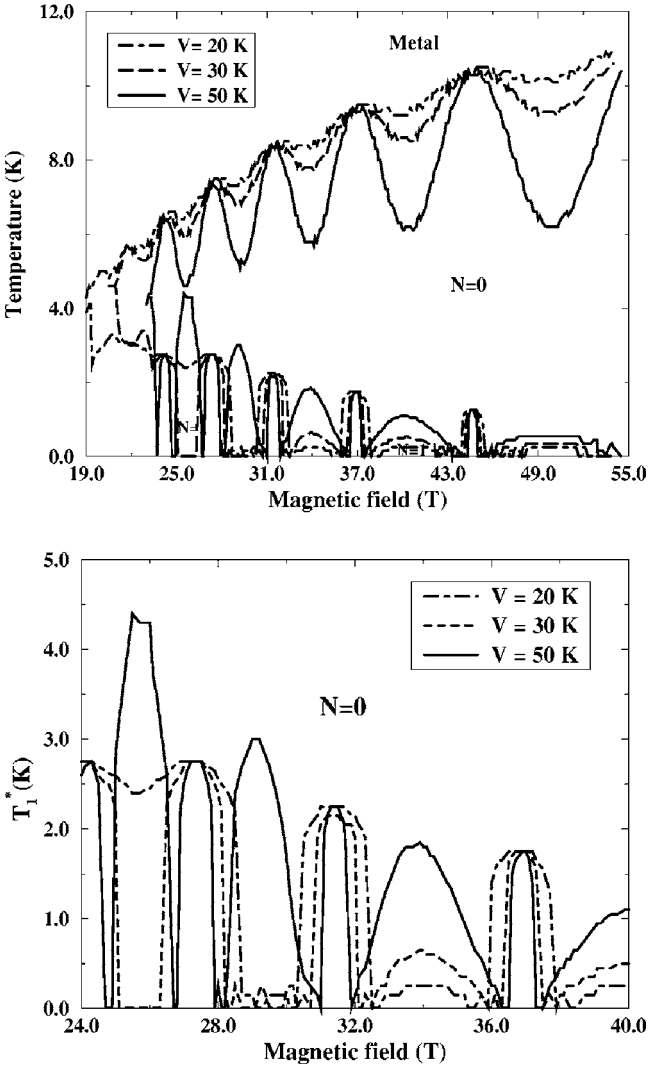

FIG. 17. (a) Temperature-field phase diagram of $(TMTSF)_2ClO_4$. For different values of the anion gap V. The calculations are done for t_b=300 K, t_b'=20 K, g_1=0.43, and g_0=0.39. The lines of the same type correspond to a given V. The set of the upper lines are ascribed to the T_0 lines while the bottom ones are associated to the T_1^* phase boundaries. The thin solid lines are the fitted curves of T_0 lines. (b) The T_1^* transition temperature in the range of 24 T to 40 T. The data are the same as in (a).

12(b)], which induces a decrease of the $N=0$ free energy [Eq. (14)].

This behavior is in agreement with the experimental results of Matsunaga *et al.*[50] who studied the effect of varying the cooling rate on the hydrogenared and deuterated $(TMTSF)_2ClO_4$. The authors have found that, with increasing the cooling rate (decreasing V), the first order phase boundary separating the last semimetallic SDW phase ($N=1$ phase in Fig. 17) from the high field insulating state ($N=0$ phase in Fig. 17) shifts toward low field region. This is in agreement with our results showing that the critical field at which T_1^* collapses is decreased with decreasing V. Matsunaga *et al.* have also found that an increase of the cooling rate furthers the insulating FISDW phase characterized by a zero Hall voltage ($N=0$ phase) but suppresses the last semimetallic phase ($N=1$ phase). The authors have then concluded that these FISDW phases correspond to different states. All these experimental features corroborate our results shown in Fig. 17.

VII. CONCLUSION

We have studied the SDW instabilities of the relaxed $(TMTSF)_2ClO_4$ in the high magnetic field regime. Based on a detailed discussion of the theoretical and experimental studies, we argued that the anion gap V, which gives rise to a two-band energy spectrum, is smaller than the hopping parameter t_b. We have, then, proposed a model where V is considered as a perturbation. The obtained results reproduce successfully the experimental features. We have shown that the highest transition temperature appearing in the high field regime corresponds to the $N=0$ phase which originates from two coexisting order parameters induced by two intraband nesting processes. These order parameters cooperate to stabilize this phase. However, their coexistence puts at disadvantage the $N=0$ phase as the magnitude of the order parameters increases with decreasing temperature. Eventually, a first order transition takes place from the $N=0$ phase to a new SDW phase which is identified as the $N=1$ state. The latter forms inside the original $N=0$ phase. This phase is induced by a single order parameter which brings into play only one nesting vector. This scenario is a different proposition compared to those existing in the literature.

We have studied the effect of some key parameters on the behavior of the FISDW states such as the coupling constants. We have shown that the coupling strengths used in the RPA expressions have to be renormalized by 1D effects in particular for large V value. We have derived the renormalization group equations for the different coupling terms. We have shown that taking into account the renormalization of the coupling constants improve the quantitative agreement between our results and the experiments.

Moreover, we have focused on the dependence of the phase diagram on the imperfect nesting parameter t_b' and the anion gap V. The results are consistent with recent experimental data. It should be stressed that the present model is not restricted to the small V limit. In particular, the scenario of two simultaneous transitions on two different bands will still hold even for large V limit. The main difference with the small V case is the method used to derive the instability criteria.

ACKNOWLEDGMENTS

This work was supported by the french-tunisian CMCU project 04/G1307. We would like to acknowledge Professor P. M. Chaikin, Professor M. J. Naughton, Dr. N. Dupuis, Dr. N. Matsunaga, Dr. D. Zanchi, Dr. D. Radić, Professor J. P. Pouget, Dr. C. Nickel, and Dr. G. Abramovici for numerous discussions at various stages of this work. We are indebted to Professor K. Murata for providing us with Ref. 44. We are grateful to Dr. J. Moser and Professor D. Jérome for discussing their unpublished data. S.H. warmly thanks Dr. A. Chalh and Dr. J. Ben Amara for helpful discussions and would like

to acknowledge the staff of Laboratoire de Physique des Solides à Orsay for kind hospitality. Numerical calculations have been carried out in Centre de Calcul El Khawarizmi in Tunis.

APPENDIX: RG EQUATIONS

In this appendix we give the RG equations of the coupling constants g_μ ($\mu=0,f,t,b$) and the hopping parameter to the first nearest neighbors t_b

$$\frac{dg_0^{(1)}(l)}{dl} = -2g_0^{(1)2} - 2g_t^{(1)}g_t^{(2)} - 2Ig_b^{(1)}(g_b^{(1)} - g_b^{(2)}),$$

$$\frac{dg_0^{(2)}(l)}{dl} = -g_0^{(1)2} - g_t^{(1)2} - g_t^{(2)2} + Ig_b^{(2)2},$$

$$\frac{dg_f^{(1)}(l)}{dl} = -2g_f^{(1)2} - 2Ig_b^{(1)}g_b^{(2)} - 2g_t^{(1)}(g_t^{(1)} - g_t^{(2)}),$$

$$\frac{dg_f^{(2)}(l)}{dl} = -g_f^{(1)2} - Ig_b^{(1)2} - Ig_b^{(2)2} + g_t^{(2)2},$$

$$\frac{dg_t^{(1)}(l)}{dl} = -2g_t^{(1)}g_0^{(2)} - 2g_0^{(1)}g_t^{(2)} - 2g_t^{(1)}(g_f^{(1)} - g_f^{(2)}) - 2g_f^{(1)}(g_t^{(1)} - g_t^{(2)}),$$

$$\frac{dg_t^{(2)}(l)}{dl} = -2g_t^{(2)}(g_0^{(2)} - g_f^{(2)}) - 2g_t^{(1)}g_0^{(1)},$$

$$\frac{dg_b^{(1)}(l)}{dl} = -2g_b^{(1)}g_f^{(2)} - 2g_f^{(1)}g_b^{(2)} - 2g_b^{(1)}(g_0^{(1)} - g_0^{(2)}) - 2g_0^{(1)}(g_b^{(1)} - g_b^{(2)}),$$

$$\frac{dg_b^{(2)}(l)}{dl} = -2g_b^{(2)}(g_f^{(2)} - g_0^{(2)}) - 2g_b^{(1)}g_f^{(1)},$$

$$\frac{d\ln \bar{t}_b(l)}{dl} = 1, \tag{A1}$$

where $\tilde{t}_b = t_b/E_0$ and

$$I = \frac{E(l)}{E(l) + 4|\Delta|}. \tag{A2}$$

Here $\Delta = VJ_0(4t_b/\omega_c)$ is the effective anion gap. The expression of I given by Fabrizio[52] is rather

$$I = \frac{E(l)}{E(l) - 4|\Delta|}, \tag{A3}$$

considering Eq. (A2) comes down to take into account three particle interaction processes during the RG procedure.[62,63,67] Such interactions have been disregarded in Ref. 52. In this RG procedure, we do not take into account the t_b' process since it is a 2D characteristic energy and is incoherent in the high temperature regime ($T \geqslant T_{\text{cross}}$).

[1] T. Ishiguro, K. Yamaji, and G. Saito, *Organic Superconductors* (Springer-Verlag, Berlin, 1998).
[2] For a recent review, see C. Bourbonnais, and D. Jérome, in *Advances in Synthetic Metals, Twenty Years of Progress in Sciences and Technology*, edited by P. Bernier, S. Lefrant, and G. Bidan (Elsevier, New York, 1999), p. 206; D. Jérome, in *Organic Conductors: Fundamentals and Applications*, edited by J.-P. Farges (Dekker, New York, 1999), p. 405.
[3] P. M. Chaikin, J. Phys. I **6**, 1875 (1996).
[4] L. P. Gor'kov and A. G. Lebed, J. Phys. (France) Lett. **45**, L433 (1984).
[5] M. Héritier, G. Montambaux, and P. Lederer, J. Phys. (France) Lett. **45**, L943 (1984); M. Héritier, G. Montambaux and P. Lederer, J. Phys. C **19**, L293 (1986).
[6] K. Yamaji, Synth. Met. **13**, 29 (1986).
[7] P. M. Chaikin, Phys. Rev. B **31**, 4770 (1985).
[8] D. Poilblanc, M. Héritier, G. Montambaux, and P. Lederer, J. Phys. C **19**, L321 (1986).
[9] K. Maki, Phys. Rev. B **33**, 4826 (1986); A. Virosztek, L. Chen, and K. Maki, Phys. Rev. B **34**, 3371 (1986).
[10] T. Vuletic, C. Pasquier, P. Auban-Senzier, S. Tomic, D. Jérome, K. Maki, and K. Bechgaard, Eur. Phys. J. B **21**, 53 (2001).
[11] A. V. Kornilov, V. M. Pudalov, Y. Kitaoka, K. Ishida, T. Mito, J. S. Brooks, J. S. Qualls, J. A. A. J. Perenboom, N. Tateiwa, and T. C. Kobayashi, Phys. Rev. B **65**, 060404(R) (2002).
[12] A. G. Lebed, Phys. Rev. Lett. **88**, 177001 (2002).
[13] M. J. Naughton, R. V. Chamberlin, X. Yan, S.-Y. Hsu, L. Y. Chiang, M. Y. Azbel, and P. M. Chaikin, Phys. Rev. Lett. **61**, 621 (1988); R. V. Chamberlin, M. J. Naughton, X. Yan, L. Y. Chiang, S.-Y. Hsu, and P. M. Chaikin, Phys. Rev. Lett. **60**, 1189 (1988).
[14] R. C. Yu, L. Chiang, R. Upasani, and P. M. Chaikin, Phys. Rev. Lett. **65**, 2458 (1990).
[15] W. Kang, S. T. Hannahs, and P. M. Chaikin, Phys. Rev. Lett. **70**, 3091 (1993).
[16] S. K. McKernan, S. T. Hannahs, U. M. Scheven, G. M. Danner, and P. M. Chaikin, Phys. Rev. Lett. **75**, 1630 (1995).
[17] U. M. Scheven, S. T. Hannahs, C. Immer, and P. M. Chaikin, Phys. Rev. B **56**, 7804 (1997).
[18] S. Uji, J. S. Brooks, M. Chaparala, S. Takasaki, J. Yamada, and H. Anzai, Phys. Rev. B **55**, 14387 (1997).
[19] J. Moser, H. Kang, W. Kang, and D. Jérome (unpublished); J. Moser, Ph.D. thesis, Orsay, 1999.
[20] O.-H. Chung, W. Kang, D. L. Kim, and C. H. Choi, Phys. Rev. B **61**, 11649 (2000).
[21] S. A. Brazovski and V. M. Yakovenko, JETP Lett. **43**, 134 (1986).
[22] A. G. Lebed and P. Bak, Phys. Rev. B **40**, R11433 (1989).

[23] T. Osada, S. Kagoshima, and N. Miura, Phys. Rev. Lett. **69**, 1117 (1992).
[24] L. P. Gor'kov and A. G. Lebed, Phys. Rev. B **51**, R3285 (1995).
[25] A. G. Lebed, Phys. Rev. B **55**, 1299 (1997).
[26] S. Haddad, S. Charfi-Kaddour, C. Nickel, M. Héritier, and R. Bennaceur, Phys. Rev. Lett. **89**, 087001 (2002).
[27] S. R. Chang and K. Maki, Phys. Rev. B **34**, 147 (1986).
[28] K. Kishigi, K. Machida, and Y. Hasegawa, J. Phys. Soc. Jpn. **66**, 2969 (1997).
[29] Y. Hasegawa, K. Kishigi, and M. Miyazaki, J. Phys. Soc. Jpn. **67**, 964 (1998).
[30] M. Miyazaki, K. Kishigi, and Y. Hasegawa, J. Phys. Soc. Jpn. **68**, 313 (1999).
[31] K. Kishigi, J. Phys. Soc. Jpn. **67**, 3825 (1998).
[32] K. Sengupta and N. Dupuis, Phys. Rev. B **65**, 035108 (2002).
[33] D. Zanchi and A. Bjeliš, Europhys. Lett. **56**, 596 (2001).
[34] D. Radić, A. Bjeliš, and D. Zanchi, Phys. Rev. B **69**, 014411 (2004).
[35] J. P. Pouget (private communication).
[36] D. Le Péleven, J. Gaultier, Y. Barrans, D. Chasseau, F. Castet, and L. Ducasse, Eur. Phys. J. B **19**, 363 (2001).
[37] L. P. Gor'kov (private communication).
[38] A. G. Lebed and N. N. Bagmet, Phys. Rev. B **55**, R8654 (1997).
[39] G. M. Danner, W. Kang, and P. M. Chaikin, Phys. Rev. Lett. **72**, 3714 (1994).
[40] See, for example, the *Proceedings on the Conference on the 20th Anniversary of Organic Superconductivity* [D. Jérome, J. Phys. IV **10**, Pr3–69 (2000); M. Grioni and J. Voit, *ibid.* **10**, Pr3–91 (2000); L. Degiorgi, V. Vescoli, W. Henderson, G. Gruner, and L. K. Montgomery, *ibid.* **10**, Pr3–103 (2000)].
[41] H. Yoshino, A. Oda, T. Sasaki, T. Hanajiri, J.-I. Yamada, S. Nakatsuji, H. Anzai, and K. Murata, J. Phys. Soc. Jpn. **68**, 3142 (1999); H. Yoshino, K. Saito, H. Nishikawa, K. Kikuchi, K. Kobayashi, and I. Ikemoto, J. Phys. Soc. Jpn. **66**, 2410 (1997).
[42] T. Osada, S. Kagoshima, and N. Miura, Phys. Rev. Lett. **77**, 5261 (1996).
[43] S. Uji, T. Terashima, H. Aoki, J. S. Brooks, M. Tokumoto, S. Takasaki, J. Yamada, and H. Anzai, Phys. Rev. B **53**, 14399 (1996).
[44] H. Yoshino, S. Shodai, and K. Murata, Synth. Met. **133–134**, 55 (2003).
[45] A. G. Lebed, and M. J. Naughton, Phys. Rev. Lett. **91**, 187003 (2003); A. G. Lebed, N. N. Bagmet, and M. J. Naughton, Phys. Rev. Lett. **93**, 157006 (2004); A. G. Lebed, H.-I. Ha, and M. J. Naughton, cond-mat/0411206 (unpublished).
[46] H.-I. Ha, A. G. Lebed, and M. J. Naughton, cond-mat/0503649 (unpublished).
[47] J. P. Pouget and S. Ravy, J. Phys. I **6**, 1501 (1996).
[48] J. P. Pouget, J. Phys. IV **10**, Pr3-43 (2000).
[49] V. M. Yakovenko, Phys. Rev. B **43**, 11353 (1991).
[50] N. Matsunaga, A. Briggs, A. Ishikawa, K. Nomura, T. Hanajiri, J. Yamada, S. Nakatsuji, and H. Anzai, Phys. Rev. B **62**, 8611 (2000); N. Matsunaga, A. Ayari, P. Monceau, A. Ishikawa, K. Nomura, M. Watanabe, J. Yamada, and S. Nakatsuji, Phys. Rev. B **66**, 024425 (2002).
[51] V. M. Yakovenko, Phys. Rev. Lett. **70**, 2657 (1993).
[52] M. Fabrizio, Phys. Rev. B **48**, 15838 (1993).
[53] D. Poilblanc, Ph.D. thesis, Université Paris-Sud, 1988.
[54] I. S. Gradshteyn and I.M. Ryzhik, *Table of Integrals, Series and Products* (Academic, New York, 1980).
[55] J. Kishine and K. Yonemitsu, J. Phys. Soc. Jpn. **67**, 1714 (1998).
[56] C. Bourbonnais, in *Proceedings of the International Summer School on High Magnetic Fields: Application in Condensed Matter Physics and Spectroscopy*, edited by C. Berthier, L. P. Levy, and G. Martinez (Springer-Verlag, Berlin, 2002), cond-mat/0204345.
[57] C. Bourbonnais and L. G. Caron, Int. J. Mod. Phys. B **5**, 1033 (1991).
[58] C. Bourbonnais, in *Strongly Interacting Fermions and High T_c Superconductivity*, Les Houches, Session LVI, 1991, edited by B. Douçot and J. Zinn-Justin (North-Holland, Amsterdam, 1991), p. 307.
[59] K. Behnia, L. Balicas, W. Kang, D. Jérome, P. Carretta, Y. Fagot-Revurat, C. Berthier, M. Horvatic, P. Ségransan, L. Hubert, and C. Bourbonnais, Phys. Rev. Lett. **74**, 5272 (1995).
[60] J. Kishine and K. Yonemitsu, J. Phys. Soc. Jpn. **68**, 2790 (1999).
[61] C. Bourbonnais (private communication).
[62] C. Nickel and G. Abramovici (private communication).
[63] G. Abramovici, C. Nickel, and M. Héritier, cond-mat/0505385, Phys. Rev. B (to be published).
[64] But they are still small enough to justify the Landau expansion at low temperature.
[65] S. Uji, S. Yasuzuka, T. Konoike, K. Enomoto, J. Yamada, E. S. Choi, D. Graf, and J. S. Brooks, Phys. Rev. Lett. **94**, 077206 (2005).
[66] Deuteration is equivalent to a chemical pressure.
[67] N. Dupuis, Eur. Phys. J. B **3**, 315 (1998).